

GUIDANCE DOCUMENT

Guidance for Using Compound Specific Isotope Analysis
(CSIA) for the Assessment of Transformation of Nitroaromatic
Explosives and RDX

SERDP Project ER-2618

MAY 2021

Dr. William A. Arnold
University of Minnesota

Dr. Thomas B. Hofstetter
**Eawag, Swiss Federal Institute of Aquatic
Science and Technology**

Dr. Neil C. Sturchio
University of Delaware

Distribution Statement A

This document has been cleared for public release



This report was prepared under contract to the Department of Defense Strategic Environmental Research and Development Program (SERDP). The publication of this report does not indicate endorsement by the Department of Defense, nor should the contents be construed as reflecting the official policy or position of the Department of Defense. Reference herein to any specific commercial product, process, or service by trade name, trademark, manufacturer, or otherwise, does not necessarily constitute or imply its endorsement, recommendation, or favoring by the Department of Defense.

REPORT DOCUMENTATION PAGE				Form Approved OMB No. 0704-0188	
Public reporting burden for this collection of information is estimated to average 1 hour per response, including the time for reviewing instructions, searching existing data sources, gathering and maintaining the data needed, and completing and reviewing this collection of information. Send comments regarding this burden estimate or any other aspect of this collection of information, including suggestions for reducing this burden to Department of Defense, Washington Headquarters Services, Directorate for Information Operations and Reports (0704-0188), 1215 Jefferson Davis Highway, Suite 1204, Arlington, VA 22202-4302. Respondents should be aware that notwithstanding any other provision of law, no person shall be subject to any penalty for failing to comply with a collection of information if it does not display a currently valid OMB control number. PLEASE DO NOT RETURN YOUR FORM TO THE ABOVE ADDRESS.					
1. REPORT DATE (DD-MM-YYYY) 26-05-2021		2. REPORT TYPE Guidance Document		3. DATES COVERED (From - To) June, 2016 - April 2021	
4. TITLE AND SUBTITLE Guidance for using Compound Specific Isotope Analysis (CSIA) for the Assessment of Transformation of Nitroaromatic Explosives and RDX				5a. CONTRACT NUMBER WQ912HQ-16-C-0014 P00001	
				5b. GRANT NUMBER	
				5c. PROGRAM ELEMENT NUMBER	
6. AUTHOR(S) William A. Arnold, Thomas B. Hofstetter, Neil C. Sturchio				5d. PROJECT NUMBER ER 2618 and ER 2726	
				5e. TASK NUMBER	
				5f. WORK UNIT NUMBER	
7. PERFORMING ORGANIZATION NAME(S) AND ADDRESS(ES) Department of Civil, Environmental, and Geo- Engineering University of Minnesota 500 Pillsbury Dr. SE Minneapolis, MN 55455				8. PERFORMING ORGANIZATION REPORT NUMBER ER-2618	
9. SPONSORING / MONITORING AGENCY NAME(S) AND ADDRESS(ES) Strategic Environmental Research and Development Program (SERDP) 4800 Mark Center Drive, Suite 16F16				10. SPONSOR/MONITOR'S ACRONYM(S) SERDP	
				11. SPONSOR/MONITOR'S REPORT NUMBER(S) ER-2618	
12. DISTRIBUTION / AVAILABILITY STATEMENT Distribution Statement A: Approved for Public Release, Distribution is Unlimited					
13. SUPPLEMENTARY NOTES					
14. ABSTRACT Methods are needed to verify that attenuation of energetic compounds, such as trinitrotoluene (TNT) and hexahydro-1,3,5-trinitro-1,3,5-triazine (RDX), in groundwater is occurring, and it must also be possible to verify that strategies to enhance degradation processes are having the desired effects. This document provides a primer on sample collection, processing, and laboratory methods for compound specific isotope analysis (CSIA) methods for nitro explosives. Data evaluation, analysis, and interpretation for both single and dual isotope fractionation is presented. Two case studies are used to demonstrate the procedures for using CSIA to support the identification of the relevant reaction process and calculate the extent of which reaction, versus dilution or sorption, is leading to decreases in concentration.					
15. SUBJECT TERMS Nitro explosives, groundwater, reduction, natural attenuation, remediation, compound specific isotope analysis					
16. SECURITY CLASSIFICATION OF:			17. LIMITATION OF ABSTRACT UU	18. NUMBER OF PAGES 57	19a. NAME OF RESPONSIBLE PERSON Dr. William Arnold
a. REPORT U	b. ABSTRACT U	c. THIS PAGE U			19b. TELEPHONE NUMBER (include area code) 612-625-8582

Standard Form 298 (Rev. 8-98)
Prescribed by ANSI Std. Z39.18

TABLE OF CONTENTS

TABLE OF CONTENTS	II
LIST OF FIGURES	IV
LIST OF TABLES	VII
LIST OF ABBREVIATIONS AND ACRONYMS	VIII
1 GENERAL INTRODUCTION.....	1
2 COMPOUND SPECIFIC ISOTOPE ANALYSIS.....	1
2.1 PRINCIPLES ^{1,2}	1
2.2 ISOTOPE EFFECTS OF THE MOST RELEVANT CHEMICAL AND BIOLOGICAL TRANSFORMATIONS OF NACs AND NITRAMINES	3
2.3 ANALYTICAL METHODS	4
2.3.1 <i>Sampling, preservation, storage</i>	5
2.3.2 <i>Analyte extraction and enrichment</i>	6
2.3.3 <i>Analyte purification and clean-up</i>	7
2.3.4 <i>Instrumental analyses</i>	7
2.3.5 <i>Standardization</i>	9
2.4 DATA EVALUATION.....	10
2.5 DATA ANALYSIS AND INTERPRETATION	12
2.5.1 <i>Calculation of isotope enrichment factors</i>	12
2.5.2 <i>Dual element isotope fractionation analysis</i>	13
3 INTERPRETATION OF STABLE ISOTOPE FRACTIONATION	13
3.1 BIOLOGICAL, CHEMICAL, AND PHOTOCHEMICAL PROCESSES.....	13
3.2 MEASUREMENT OF ENRICHMENT FACTORS IN LABORATORY EXPERIMENTS	14
3.3 MULTI-ELEMENT ISOTOPE FRACTIONATION	16
3.4 APPLICATION OF CSIA TO FIELD SAMPLES: CASE STUDIES.....	23
3.4.1 <i>Iowa Army Ammunition Plant (IAAAP)</i>	23
3.4.2 <i>Pantex Plant</i>	28
3.5 USING CSIA RESULTS TO AID IN INTERPRETATION OF FIELD DATA	33
4 CONCLUSIONS AND RECOMMENDATIONS.....	35
5 REFERENCES.....	37
APPENDIXA.....	A-1

LIST OF FIGURES

Figure 1. Survey of the *initial steps* of the most important (bio)transformation processes of NACs and RDX for which some isotopic characterization exists. Reactions labelled in green, red, and blue color represent reductive, oxidative, and substitution/elimination reactions, respectively. Further transformation is contingent upon the specific reaction conditions..... 4

Figure 2. Survey of the generalized stable isotope analysis workflow from sampling to isotope ratio measurements of nitroaromatic and nitramine compounds in aqueous or solid matrices as well as for pure compounds. Abbreviations used include SPME (solid-phase microextraction), SPE (solid phase extraction), LL (liquid-liquid extraction), ASE (accelerated solvated extraction), GC/IRMS (gas chromatograph coupled to isotope ratio mass spectrometer), LC/IRMS (liquid chromatography/IRMS), EA/IRMS (elemental analysis/IRMS)..... 5

Figure 3. Determination of method quantification limits (MQL) for N and C isotope analysis of DNAN by SPME-arrow-GC/IRMS. Panels (a) and (b) show data for $\delta^{15}\text{N}$ and $\delta^{13}\text{C}$, respectively. Dashed lines indicate the total uncertainty used for MQL determination as well as one standard deviation of the reference isotope signatures determined by EA/IRMS..... 11

Figure 4. Determination of method quantification limits (MQL) for N and C isotope analysis of RDX by SPME-arrow-GC/IRMS. Panels (a) and (b) show data for $\delta^{15}\text{N}$ and $\delta^{13}\text{C}$, respectively. 11

Figure 5. Nitrogen isotope signatures, $\delta^{15}\text{N}$, versus fraction of unreacted RDX (c/c_0) determined in experiments with various Fe(II) containing suspensions. The goethite data represent experiments with Fe(II)/goethite at pH 7.0 and pH 7.5, and Fe(II)/goethite with Elliot Soil Humic Acid (ESHA) at pH 7.5, and all other experiments were carried out at pH 7.5. The curve was fit using the data from each set of conditions to obtain a single ϵ_{N} value of $-7.4 \pm 0.2\text{‰}$ (individual values in Tong et al.⁵³). The error band shows the 95% confidence interval. 15

Figure 6. Nitrogen enrichment factors during RDX collected from this study and adapted from previous research under varying experimental conditions. (a) Bernstein et al.;¹⁷ Fuller et al.;²⁵ (b) Fuller et al.;²⁵ (c) this study; (d) Gelman et al.²⁴ Error bars represent the 95% confidence intervals..... 15

Figure 7. Initial steps for the transformation of 2,4-dinitroanisole (1) by (a) alkaline hydrolysis through nucleophilic aromatic substitution to 2,4-dinitrophenol (6). Compounds 2 to 5 are resonance structures of the Meisenheimer complex intermediates.⁵⁴ (b) Hypothesized enzymatic hydrolysis of DNAN by *Nocardioide*s sp. JS1661 and enzyme assays containing DNAN *O*-demethylase. Compound 7 shows one of several possible transition states for a hydrolytic *O*-demethylation at the aliphatic C atom of the methoxy group. 16

Figure 8. C and N isotope fractionation associated with the transformation of DNAN to DNP by alkaline hydrolysis at pH 12 (panels a and b) and during biodegradation by *Nocardioide*s sp. JS1661 (panels c and d). Panels (a) and (b) show $\delta^{13}\text{C}$ of DNAN and DNP vs. fraction of remaining DNAN, c/c_0 ; panels (c) and (d) show the corresponding $\delta^{15}\text{N}$ trends. Lines represent fits of C isotope fractionation (equations 1 and 2) for DNAN and DNP with different

assumptions for intramolecular $\delta^{13}\text{C}$ distribution among aromatic and aliphatic C atoms in panel (a). The solid and dotted lines are nonlinear fits to the substrate and product isotope fractionation, respectively. The shaded areas indicate the 95% confidence intervals. 17

Figure 9. Reduction of DNAN to nitroso (2) and hydroxylamine (3) intermediates. Complete reduction of the first nitro group results in 2-amino-4-nitroanisole (4; 2-ANAN) or 4-amino-2-nitroanisole (4-ANAN) and reduction of both nitro groups results in 2,4-diaminoanisole (DAAN). 18

Figure 10. Nitrogen ($\delta^{15}\text{N}$) and carbon ($\delta^{13}\text{C}$) isotope signatures vs fraction of remaining substrate (c/c_0) during DNAN reduction by iron-bearing minerals. Solid lines represent fits from nonlinear regression with shaded portions indicating the 95% confidence intervals. Dashed lines designate 95% prediction intervals. N and C isotope enrichment factors (ϵ_{N} , ϵ_{C}) were determined from non-linear regression of the data points for each mineral type. Data are shown for untreated materials in the presence of Fe(II) and dithionite-treated materials. 18

Figure 11. Dual-element (N vs C) isotope analysis to indicate multiple potential DNAN transformation pathways.^{21,52} Data from the present study for abiotic reduction by untreated minerals + Fe(II) (stars) and from columns receiving in situ chemical reduction (ISCR) (hexagons) are shown. The dotted line represents the fit from linear regression by the York method as described by Ojeda et al.⁴⁸ The isotope fractionation observed during biodegradation (circles) and alkaline hydrolysis (diamonds) are provided for reference. Shaded portions represent the 95% confidence intervals from nonlinear regression analysis. 19

Figure 12. $\delta^{13}\text{C}$ of RDX vs. signal amplitude for RDX standard injections performed during the analysis of RDX samples from RDX reduction experiments in Fe(II)/hematite and green rust suspensions (red/green symbols). The grey area delineates the amplitude range of constant $\delta^{13}\text{C}$ for RDX standard measurements. 20

Figure 13. Carbon isotope fractionation of RDX in reduction experiments in suspensions of green rust (panel a) and Fe(II)/hematite (panel b). ϵ_{C} - values and initial RDX C isotope signatures ($\delta^{13}\text{C}_0$) were obtained from non-linear regression. Parameter uncertainties and shaded areas represent 95% confidence intervals. 21

Figure 14. Correlation of C and N isotope fractionation of RDX reduction in suspensions of green rust (panel a) and Fe(II)/hematite (panel b) Error bars are standard deviations of triplicate C and N isotope ratio measurements, shaded are indicate 95% confidence intervals of the linear regression. 22

Figure 15. $\Delta\delta^{13}\text{C}$ (‰) and $\Delta\delta^{15}\text{N}$ (‰) in DNAN during photolysis under UV-A (~350-nm) and UV-C (~250-nm) irradiation. Initial DNAN isotope composition: $\delta^{13}\text{C} = -37.2$ ‰ and $\delta^{15}\text{N} = -2.5$ ‰. Dashed gray lines are 95% confidence intervals of the linear regressions (from ref⁶⁰). 23

Figure 16. Local map of IAAAP monitoring wells sampled RDX analysis. Ground water contours are labelled with 207 m and 204 m. Lines without labels are tributaries and drainages ditches. 24

Figure 17. Evaluation of RDX concentrations and $\delta^{15}\text{N}$ values with regard to reductive transformation in monitoring wells along Line 800 at IAAAP (map see Figure 16). The samples are sorted according to increasing distance from the operationally defined contamination source well G-20. (a) Aqueous concentrations of RDX at different sampling locations including calculated extent of RDX reduction (eq. 5) based on the ϵ_{N} -value obtained in laboratory batch experiments with Fe-minerals. (b) $\delta^{15}\text{N}$ values of RDX at different sampling locations. (c) Concentrations of partially reduced RDX reduction products..... 26

Figure 18. Map of the study site, indicating key topographic features and wells sampled. Colors designate three transects. The dash lined represents the 2 $\mu\text{g/L}$ RDX contour in 2015 (from ref ¹⁵)..... 28

Figure 19. Detected concentrations of explosives and breakdown products in groundwater at the Pantex study site. A) RDX; B) Sum of nitroso-containing RDX breakdown products; C) NDAB (from ref ¹⁵)..... 30

Figure 20. A) Summary of RDX $\delta^{15}\text{N}$ results. The RDX concentration contour surface is shown for reference. B) $\delta^{15}\text{N}$ values of RDX as a function of the distance from the center of Playa 1. Symbols represent wells in immediate vicinity of Playa 1 (squares), near the location of RDX source release into the ditch (triangles), or in the southeastern region of the current plume (circles) (from ref ¹⁵)..... 31

Figure 21. Proposed workflow for the use of CSIA to support identification of nitro explosive degradation reaction and estimation of the extent of transformation attributable to the specified reaction..... 34

LIST OF TABLES

Table 1. Representative enrichment factors and kinetic isotope effects for explosives. ^{6,52,53,56–61} A complete listing for various NACs and explosives is given in Appendix A.....	22
Table 2. Chemical data from the collected groundwater samples from the Iowa Army Ammunition Plant.	27
Table 3. Summary of detections of RDX, RDX breakdown products, $\delta^{15}\text{N}$ values of RDX and other explosives in groundwater collected for the Pantex study. ND = Not detected or no data. Data is from ref. ¹⁵	32

LIST OF ABBREVIATIONS AND ACRONYMS

Acronym	Definitions
AKIE	Apparent kinetic isotope effect
2-ANAN	2-amino-4-nitroanisole
4-ANAN	4-amino-2-nitroanisole
ASE	Accelerated solvent extraction
C, ¹³ C, ¹² C	Carbon, carbon 13 isotope, carbon 12 isotope
<i>c</i> and <i>c</i> ₀	concentration and initial concentration
CSIA	compound specific isotope analysis
DAAN	2,4-diaminonitroanisole
DCM	dichloromethane
DNAN	2,4-dinitroanisole
DNP	Dinitrophenol
DNX	1,3-dinitroso-5-nitro-1,3,5-triazacyclohexane
E	Element E
^h E	Heavy isotope of element E
^l E	Light isotope of element E
<i>E</i> _H	Electrochemical potential
EA	Elemental analysis
<i>f</i>	Fraction of substance remaining (<i>c/c</i> ₀)
<i>F</i>	extent of parent compound transformation (1- <i>c/c</i> ₀)
Fe	Iron
ft. bgs	Feet below ground surface
GC	gas chromatography
H	Hydrogen
<i>h</i>	Heavy isotope
HMX	1,3,5,7-Tetranitro-1,3,5,7-tetrazocane
IAAAP	Iowa Army Ammunition Plant
IRMS	isotope ratio mass spectrometry
ISCR	In situ chemical reduction
KIE	kinetic isotope effect
<i>k</i>	Reaction rate constant
<i>l</i>	Light isotope
LC	Liquid chromatography
LL	Liquid-liquid (extraction)
MNX	hexahydro-1-nitroso-3,5-dinitro-1,3,5-triazine
MQL	Method quantification limit
<i>n</i>	Number of reactive atoms of a particular element
N, ¹⁵ N, ¹⁴ N	Nitrogen, nitrogen 15 isotope, nitrogen 14 isotope
NAC	nitroaromatic compound
NDAB	4-nitro-2,4-diazabutanal
NMR	Nuclear magnetic resonance
PTFE	Polytetrafluoroethylene
PTV	programmed temperature vaporization

RDX	hexahydro-1,3,5-trinitro-1,3,5-triazine
SPE	Solid phase extraction
SPME	Solid phase microextraction
TAFB	Tinker Air Force Base
TCAAP	Twin Cities Army Ammunition Plant
TNT	2,4,6-trinitrotoluene
TNX	hexahydro-1,3,5-trinitroso-1,3,5-triazine
$\delta^{13}\text{C}$	C-isotope signature
$\delta^{15}\text{N}$	N-isotope signature
$\delta^{\text{hE}}, \delta^{\text{hE}_0}$	Isotope signature if element E with isotopologue atomic mass h. Subscript 0 indicates initial value.
$\Delta^{13}\text{C}$	Change in C-isotope signature
$\Delta^{15}\text{N}$	Change in N-isotope signature
ϵ_{C}	C isotope enrichment factor
ϵ_{E}	Element E isotope enrichment factor
ϵ_{N}	N isotope enrichment factor
Λ_{E_1/E_2}	Correlation slope between element 1 and element 2 isotope fractionation

1 GENERAL INTRODUCTION

Nitro explosives are common groundwater contaminants at explosive manufacturing and testing sites. Nitro explosives include nitroaromatic compounds (NACs), such as the traditional explosive trinitrotoluene (TNT) and the insensitive munitions compound 2,4-dinitroanisole (DNAN), as well as nitramine structures such as 1,3,5-trinitro-1,3,5-triazine (RDX) and 1,3,5,7-tetranitro-1,3,5,7-tetrazocine (HMX), and other structures such as nitrotriazolone (NTO). The compounds are moderately to extensively soluble in water, and thus transport off site is a substantial concern. Various hydrolytic, biological, and abiotic transformation processes of nitro explosives are known and have been proposed as a means to degrade these compounds in both engineered and natural attenuation scenarios for remediation. However, decreasing concentration may not be sufficient to verify that contaminant mass is being reduced and identify the process responsible. Additionally, the lengthy time scales over which (bio)degradation occurs, and complicating factors such as multiple contamination sources, dilution and sorption processes, and subsurface heterogeneity make assessment of remediation success challenging. Additional data, such as identification of reaction products or quantification of specific genes known to facilitate biodegradation offer additional support in identifying reaction processes but not the extent of reaction. The application of compound specific isotope analysis (CSIA), in which stable isotope ratios (e.g., $^{13}\text{C}/^{12}\text{C}$, $^{15}\text{N}/^{14}\text{N}$) in the pool of remaining parent compounds are measured along a groundwater flow path, offers the potential to assess the extent of contaminant transformation and identification of the process(es) responsible for observed decrease in concentration. Robust use of CSIA requires understanding of isotope enrichment factors for various possible reactions, robust analytical protocols, and careful data interpretation.

2 COMPOUND SPECIFIC ISOTOPE ANALYSIS

2.1 Principles^{1,2}

The kinetics of chemical reactions are often a function of the strength of the bond broken or formed. The bond strength is a function of several factors, one of which is the atomic weight of the elements in the bond. Because atoms have different isotopes, the rate of reaction is affected by the isotope present, with the heavier isotopes usually reacting more slowly. This gives rise to the kinetic isotope effect (KIE), which is a ratio of the rate constants (k) of the light and heavy isotopes for an element of interest (E):

$$\text{KIE} = \frac{k_l}{k_h} \quad (1)$$

where l represents the light isotope and h the heavy isotope (e.g., ^{12}C and ^{13}C , respectively). Primary KIEs are changes due to the isotopes present at the bond that is breaking or forming. The values are often greater than one, with KIEs being of order 1.02 to 1.10 for atoms other than hydrogen. Values for hydrogen are as high as eight. Secondary effects are due to isotopes present

at bonds other than the one breaking or forming, and these effects are typically much smaller than the primary effects.

The abundance of the heavy isotope in element E is quantified and reported as difference in per mil (‰) $\delta^h\text{E}$ with respect to an international reference standard for that element.

$$\delta^h\text{E} = \left(\frac{\left(\frac{{}^h\text{E}}{{}^l\text{E}} \right) - \left(\frac{{}^h\text{E}}{{}^l\text{E}} \right)_{\text{ref}}}{\left(\frac{{}^h\text{E}}{{}^l\text{E}} \right)_{\text{ref}}} \right) \times 1000 \text{ ‰} \quad (2)$$

or

$$\delta^h\text{E} = \frac{\left(\frac{{}^h\text{E}}{{}^l\text{E}} \right)_{\text{sample}} + 1}{\left(\frac{{}^h\text{E}}{{}^l\text{E}} \right)_{\text{standard}} + 1} - 1 \quad (3)$$

Because the light isotopes (generally) react more quickly, the pool of reactant becomes enriched in the heavier isotopes over time. This enrichment is quantified using an enrichment factor (ϵ_E , units of ‰):

$$\frac{\delta^h\text{E} + 1}{\delta^h\text{E}_0 + 1} = \left(\frac{c}{c_0} \right)^{\epsilon_E} = f^{\epsilon_E} \quad (4)$$

$\delta^h\text{E}_0$ is the isotope signature of unreacted substrate for the element of interest, and c/c_0 is the fraction of remaining substrate, also termed f . This is alternatively expressed as the extent of reaction (F):

$$F = 1 - \frac{c}{c_0} = 1 - \left(\frac{\delta^h\text{E} + 1}{\delta^h\text{E}_0 + 1} \right)^{\frac{1}{\epsilon_E}} \quad (5)$$

Thus, if the isotope enrichment factor for a specific process is known, and isotope ratios at two points in time (or space) are measured, the extent of transformation can be calculated.

Apparent kinetic isotope effects (AKIEs) are then from the calculated ϵ_E values:¹

$${}^h\text{E-KIE} = \frac{1}{1 + n \cdot \epsilon_E} \quad (6)$$

In equation 6, n is the number of atoms of element E that lead to dilution of the isotopic signal. Because these effects are specific to a particular reaction process, quantifying the changes in the

abundance of isotopes in the reactant (and product) pools is a means to identify which reaction process is occurring in environmental systems when concentrations of a pollutant are decreasing. Processes that lead to lower aqueous concentrations but do not involve reaction, such as sorption and dilution, are non-fractionating, and thus monitoring the changes in isotope abundance allows assessment of whether or not the decreasing concentration is due to a reactive process. Because the isotopic enrichment is dependent on the specific bonds being broken, it is possible to use changes in isotope ratios to not only validate that a reaction is occurring, but also which reaction process is occurring. To this end, the correlation of isotope fractionation from different elements E_1 and E_2 , Λ_{E_1/E_2} , is also useful to characterize how a contaminant is transformed.

$$\Lambda_{E_1/E_2} = \frac{\Delta E_1}{\Delta E_2} \approx \frac{\varepsilon_{E_1}}{\varepsilon_{E_2}} \quad (7)$$

2.2 Isotope effects of the most relevant chemical and biological transformations of NACs and nitramines

Assessing the transformation of NACs or nitramines in the environment is complicated by the possibility of several simultaneous (and potentially competing) transformation and transport processes (e.g., sorption, volatilization, (bio)degradation). Likewise, NACs in the subsurface may be present in different phases and exhibit high soil and sediment sorption, rendering the interpretation of concentration dynamics difficult. Because these non-reactive processes minimally affect the isotopic compositions of explosives, their chemical and biological transformations can be assessed by change of the residual stable isotope composition.^{3,4}

In recent years, most of the relevant (bio)degradation processes have been characterized in terms of isotope effects and isotopic enrichment factors. Figure 1 shows the initial reaction steps of reductive, oxidative and substitution/elimination reactions. These steps allow for the derivation for some rules-of-thumb regarding the best elements for tracking these processes by CSIA: (1) most reductive reactions involve transformation of a NO_2 group to a more reduced form (e.g., nitroso or amino groups) – those reactions are accompanied by large (i.e., primary) N isotope fractionation whereas the associated isotope effects for C and H are only secondary and therefore smaller; and (2) oxidative transformation, by contrast, is often simply oxygenation of the carbon backbone of the molecule – therefore, C and H isotope fractionation is moderately large for these processes whereas N isotope fractionation is quite small.

Key aspects of the implementation of CSIA for field samples are 1) proper collection, preservation and storage of samples; 2) if necessary, analyte extraction and enrichment; 3) proper analytical methods, with assessment of detection limits and concentration effects on instrument response/calibration; and 4) protocols for data analysis and interpretations.

The utility of CSIA relies on measurement of isotope enrichment factors in the laboratory in a way that field data can be interpreted. Section 3 of this document presents some examples of these measurements and the factors that need to be considered when designing laboratory

experiments to determine isotope enrichment factors. It is crucial to understand how robust these values are for different chemical/microbial systems.

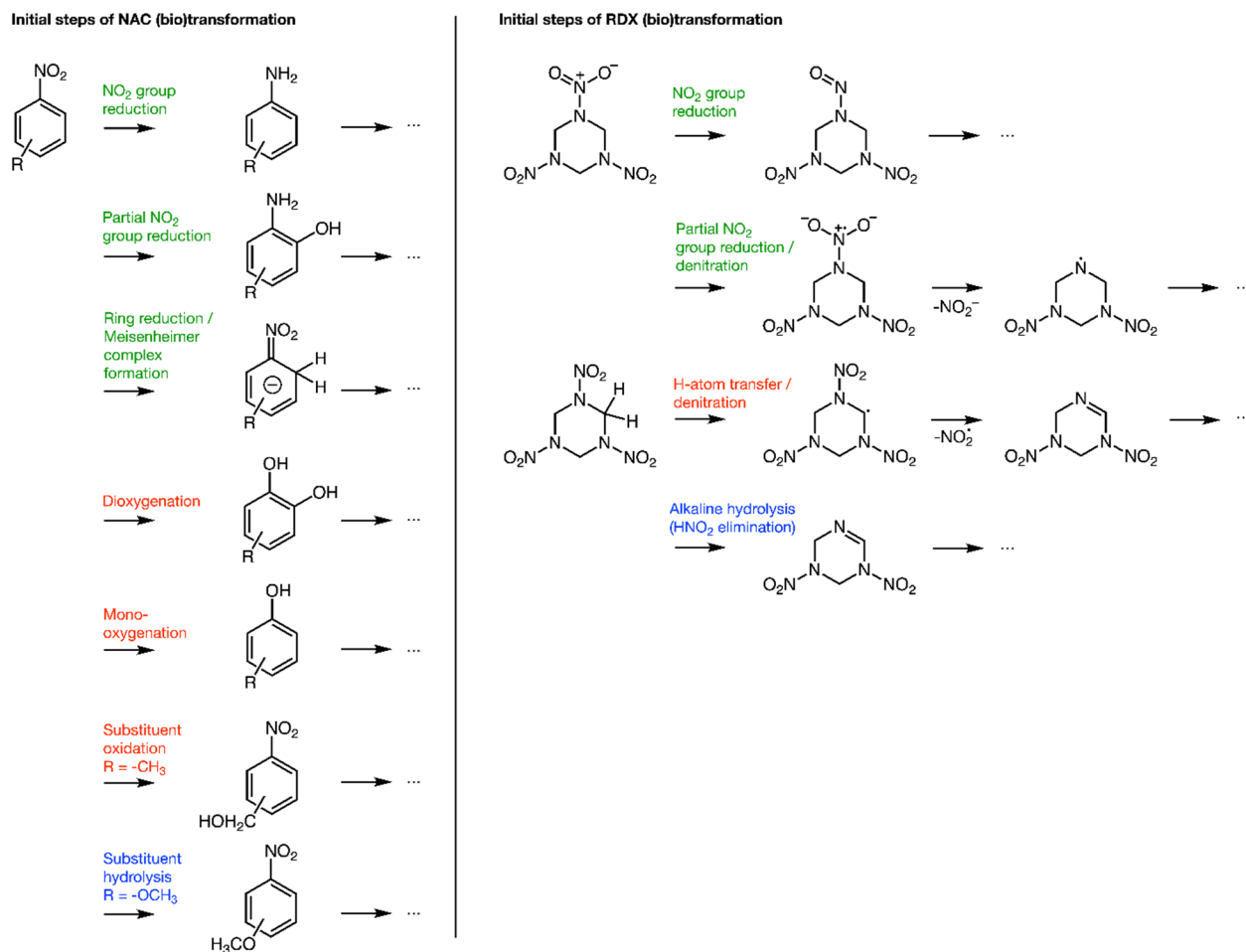


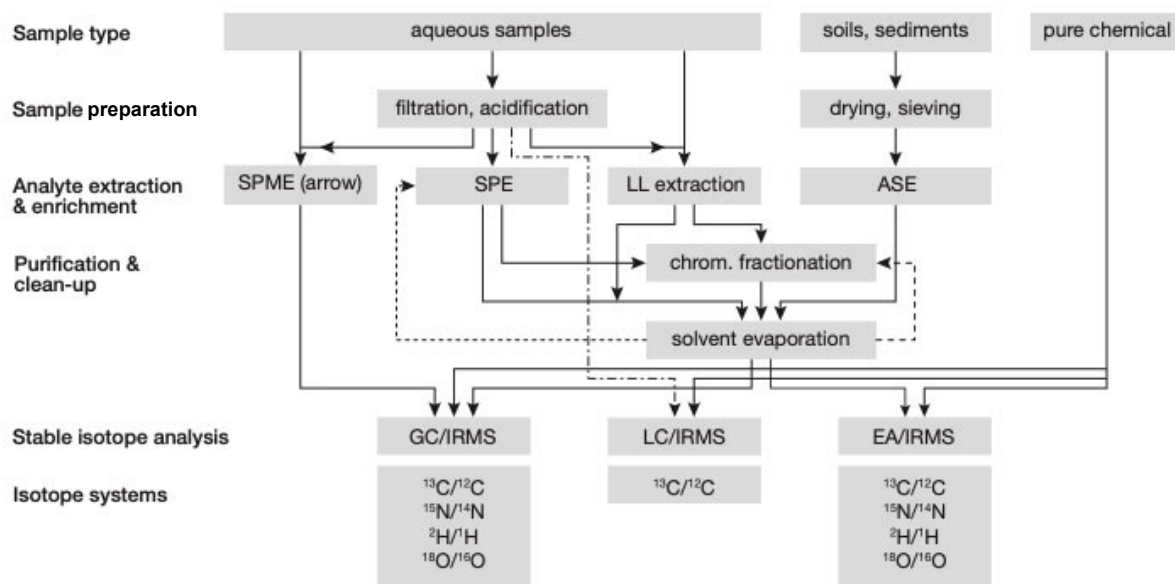
Figure 1. Survey of the *initial steps* of the most important (bio)transformation processes of NACs and RDX for which some isotopic characterization exists. Reactions labelled in green, red, and blue represent reductive, oxidative, and substitution/elimination reactions, respectively. Further transformation is contingent upon the specific reaction conditions.

2.3 Analytical methods

Procedures for stable isotope analysis of NACs and nitramines depend on the matrix in which the analyte is present, its concentration therein, and on the instrumentation available. Figure 2 provides a simplified overview of the most popular workflows for these compounds. CSIA performed by gas chromatography/isotope ratio mass spectrometry (GC/IRMS) is the most popular approach because of its superiority in terms of analyte separation compared to liquid chromatography (LC)/IRMS or elemental analysis (EA)/IRMS. Contaminant polarity, however,

can limit the amenability of certain analytes to gas chromatography thus making the use of alternative methods necessary.

The following sections, describe the most frequently applied procedural steps for sample preparation, analyte extraction and enrichment, purification steps, and the most relevant factors



for instrumental analysis from the perspective of analyses of NACs. Specific references to procedures of nitramines are given if they go beyond previous documentations for RDX.⁵

Figure 2. Survey of the generalized stable isotope analysis workflow from sampling to isotope ratio measurements of nitroaromatic and nitramine compounds in aqueous or solid matrices as well as for pure compounds. Abbreviations used include SPME (solid-phase microextraction), SPE (solid phase extraction), LL (liquid-liquid extraction), ASE (accelerated solved extraction), GC/IRMS (gas chromatography coupled to isotope ratio mass spectrometer), LC/IRMS (liquid chromatography/IRMS), EA/IRMS (elemental analysis/IRMS).

2.3.1 Sampling, preservation, storage

Field Sample Collection and Processing

Sample collection and processing steps are typically accompanied by a quantification of mass recoveries from the addition of standards to the environmental matrices being studied. For CSIA, those standards should ideally consist of compounds of known isotopic composition, typically in-house isotopic standards to evaluate sample-processing related isotopic fractionation (see example in Wjker et al.⁶). A wide array of NACs such as chlorinated or methylated nitrobenzenes have been tested with CSIA^{6,7} and such in-house standards are typically characterized as pure substances by EA/IRMS versus internationally accepted standard materials⁸ or versus organic reference materials available for CSIA.^{9,10}

Water Samples

Groundwater samples can be collected in the field into pre-cleaned bottles, stored on ice, and shipped to the laboratory for processing and extraction. The first step is using pre-combusted glass fiber filters to remove particles. Preservation of the samples via acidification to pH values between 2 and 4 can be used to minimize homogeneous loss processes such as base-catalyzed hydrolysis and abiotic reduction, and to inhibit biological activity. Storage at 4 °C has been shown to preserve the original isotopic composition of NACs.

Solid Materials

Soils contaminated with NAC explosives should be dried at 25 °C in a drying cabinet to a constant weight. Thereafter, soil specimens are ground with a jaw crusher and rotor mill, sieved to <5 mm, and mixed thoroughly. Samples on the order of tens of grams of dried soil material are used for further processing by accelerated solvent extraction (ASE).⁶ Processed soil samples should be stored at 4 °C in the dark.

2.3.2 Analyte extraction and enrichment

Aqueous samples

NACs can be extracted from small water samples (1-10 mL) and enriched on sorbent materials by direct immersion solid-phase microextraction (SPME, Figure 2).^{7,11,12} Sorbent materials typically include polyacrylate, carbowax-divinylbenzene, and carboxen-divinylbenzene, and allow for accurate determination of C and N isotope ratios in concentration ranges between 10-200 µM. A modified version of SPME, SPME arrow, enables lower method quantification limits in the sub-µM range.¹³ Extraction conditions typically include 45 minute extraction in solutions containing 4 M NaCl at 40 °C followed by thermal desorption in a split/splitless injector at 270 °C. Alternatively, DNAN, and potentially other NACs, can be extracted from water into ethyl acetate (1:1 vol/vol) using ultrasound-assisted liquid-liquid extraction, followed by evaporation of the ethyl acetate to concentrate DNAN for GC-IRMS analysis.¹⁴

Larger sample volumes and lower NAC concentrations are accessible through solid-phase extraction (SPE). Typical procedures use PorapakTM RDX cartridges as described by Wijker et al.⁶ SPE-cartridges are conditioned with 20 mL of dichloromethane and 20 mL of Milli-Q[®] water before loading aqueous solutions containing the NACs. Loaded cartridges are washed with Milli-Q[®] water and air-dried and analytes eluted with 5 mL of dichloromethane. Traces of water in the organic phase are removed through the addition of anhydrous Na₂SO₄ followed by filtration through a 0.22 µm hydrophobic polytetrafluoroethylene (PTFE) filter. Depending on the target concentration for isotopic analyses, samples can be further evaporated under a stream of N₂.

RDX is enriched by SPE using SupelcleanTM ENVITM-Chrom P SPE cartridges (Sigma Aldrich) that are conditioned sequentially with 3 mL of ethyl acetate, methanol, and ultrapure water prior to loading 20 mL of sample onto each cartridge by gravity. The cartridges are then vacuum-dried and eluted with two 3 mL portions of ethyl acetate, such that minimal water is present in the eluent. Samples are then dried with sodium sulfate, filtered with TeflonTM syringe filters (0.2

μm), and evaporated to 0.2 mL for stable isotope analyses. Acetonitrile has also been used to extract RDX from the SPE cartridges.^{5,15} Note that after loading and vacuum drying, the SPE cartridges can be stored at 4 °C for weeks before elution and analysis. Alternative SPE methods include extraction with solid-phase extraction disks¹⁶ with slightly different conditioning of the sorbent materials were applied to enrich RDX from groundwater samples of up to 8 L. For laboratory experiments, RDX has also been enriched by liquid-liquid extraction into dichloromethane (DCM).¹⁷ Periodic GC-IRMS and EA-IRMS analyses of a DNAN/ethyl acetate in-house isotopic reference solution performed over a period of three years showed no significant long-term change in the C and N isotopic composition of DNAN. The EA-IRMS measurements were done on dry DNAN after evaporation of the solvent.

Soil samples

NACs can be extracted from soil samples following a multi-step procedure.⁶ To that end, 10 to 20 g of dried and sieved materials were extracted with ASE (Dionex™ ASE 350). Each of the 10 mL extraction cells were equipped with glass and cellulose filters, filled with soil, and mixed with 1 g of diatomaceous earth as a dispersing agent. The ASE-cells were loaded into the extraction oven, filled with acetone, and preheated for 5 minutes followed by a 5 minute static extraction at 100 °C. The extracts are evaporated under a stream of N₂ to 1 mL and filtered through a 0.22 μm hydrophobic PTFE filter. Extracts were cleaned further by dissolution in 1 L of Milli-Q® water followed by SPE as described above. Note that each of the sample preparation steps was evaluated for method-induced stable isotope fractionation. Changes of C and N isotope ratios were usually within the total uncertainty of the instrumental measurement.

RDX from soil samples has also been extracted by suspension of soil materials in distilled water for 24 hours followed by centrifugation of the solid material. RDX in the supernatant is then extracted with SPE disks as described above for water samples.

2.3.3 Analyte purification and clean-up

Clean-up of analytes after enrichment steps can be necessary to remove carbon and nitrogen-containing matrix compounds. Those steps are typically combined with some degree of evaporation of the solvent under a stream of N₂ to samples of 0.5 to 1.0 mL to achieve the concentrations necessary for accurate instrumental analysis as described below.

RDX from liquid-liquid extraction into DCM has been separated from interfering compounds by thin-layer chromatography. The ability to withdraw silica gel-enriched samples that are later dissolved in DCM enables the analysis of ¹⁵N/¹⁴N ratios by elemental analysis/IRMS.¹⁸

2.3.4 Instrumental analyses

The stable isotope ratios ¹⁵N/¹⁴N, ¹³C/¹²C, and ²H/¹H of NACs and RDX are typically analyzed by GC/IRMS/because this instrumental setup is most versatile in terms of sample injection combined with analyte enrichment and it is currently the method of choice for CSIA of volatile and semivolatile organic compounds. Polar compounds not separable by GC may first be

derivatized to a GC-separable species to enable isotopic analysis by GC/IRMS. Alternatively, these may be analyzed by liquid chromatography coupled with IRMS (LC/IRMS), although this method is routinely used only for measurement of C isotope ratios.¹⁹ Procedures for direct immersion SPME of *aqueous samples* of NACs require specification of extraction time (e.g., 45 minutes), temperature (40 °C), NaCl concentration (4.0 M), and desorption time (3 minutes) where analytes are desorbed from the SPME fiber at 270 °C in a split/splitless injector equipped with a deactivated liner.⁷ *Liquid samples* of NACs are injected in organic solvents such as ethyl acetate and DCM with injection volumes of 1 µL. Larger volumes are possible depending on the solvent type used as found for analytes other than explosives.²⁰

A possible setup used for NACs includes separation of NACs on an RtxTM-5MS capillary column (0.32 mm ID, 1 µm film thickness, 30 m length) and operated in splitless mode (splitless time six minutes, purge flow 50 mL/min) with the following temperature program: 50 °C for one minute, ramp 10 °C min⁻¹ to 250 °C, hold for five minutes.²¹

Conversion of NACs to analyte gases for isotopic analysis can be accomplished by typical combination of commercial combustion Ni/Cu/Pt furnaces with Cu-based reduction reactors. However, most C and N isotope ratio measurements on NACs were carried out with a customized Ni/Pt reactor that requires frequent re-oxidation but exhibits excellent long-term performance and reproducibility.²² Note that according to more recent evidence, ²H/¹H ratio measurements should be carried out using high-temperature conversion reactors with elemental Cr; this is especially important for halogenated compounds.²³

Isotopic analysis of C and N of RDX requires alternative instrument settings to account for possible RDX decomposition.^{24,25} Typically 1-2 µL volume of an ethyl acetate solution are injected into a programmed temperature vaporization injector (PTV) at an injection temperature of 180 °C. Following a splitless time of one minute (flow 50 mL/min), the injection temperature is raised to 300 °C for the remainder of the run to remove any residual analytes from the injector. Gas chromatography can be performed with identical column material as NACs and a suitable temperature program is one minute at 50 °C, 15 °C/min to 180 °C, 45°C/min to 250 °C (15-minute hold). Note that decomposition of RDX during analyte transfer and conversion on an IRMS system leads to peak broadening that, depending on the sample matrix can lead to interference with C-containing compounds making it more difficult to obtain an acceptable linear range for $\delta^{13}\text{C}$ measurements.^{17,24}

The C and N isotope ratios of pure and purified NACs and RDX are routinely measured by EA/IRMS. These measurements follow standard procedures where the samples are introduced in tin capsules to silvered cobaltous/cobaltic oxide and chromium oxide containing combustion reactors and Cu-based reduction reactors operated at the usual temperatures.²⁶

A relatively recent development in CSIA is the application of carbon 13 isotope nuclear magnetic resonance (¹³C-NMR) to measurement of position-specific C isotope ratios in organic

pollutants.^{27,28} This method was applied to determine the position-specific ^{13}C distribution in DNAN and showed substantial enrichments in ^{13}C at the C2 and C4 positions, as well as a large ^{13}C depletion in the C7 (methoxy group) position.²⁹ Unfortunately, the ^{13}C -NMR measurement requires a large amount of material (~200 mg) and is therefore practical mainly for laboratory studies.

A more recent development in CSIA that shows tremendous promise is the application of Orbitrap high-resolution mass spectrometry to the isotopic analysis of organic molecules.^{30,31} This instrumentation can be coupled with GC or LC sample introduction methods, and the sensitivity and precision is comparable to GC/IRMS methods. However, its principal advantage is that it allows the relative proportions of whole-molecule isotopologs to be measured, thus precluding the requirement of compound conversion to simple gases (CO_2 , N_2 , CO , H_2) that are normally produced for GC/IRMS measurements. In principle, the Orbitrap technology is capable of simultaneous measurement of H, C, N, O, S, and Cl isotope ratios in intact molecules, and it may eventually become an important tool for CSIA of explosive compounds and their degradation products in the environment.

2.3.5 Standardization

Measured isotope ratios are referenced to standard materials to ensure comparability among measurements across laboratories and enhance quality assurance. The typical strategy includes the use of certified standard materials as well as calibrated in-house standards for frequent use.^{32,33} Explosives, however, are rarely available and not necessarily at the high purity required for isotopic analyses. To that end, alternative chemicals are recommended for standardization. For $\delta^{13}\text{C}$ and $\delta^{15}\text{N}$ measurements by EA/IRMS, glutamic acids of USGS40 and USGS41 have been used as reference materials against which in-house materials are calibrated over a range of 60‰ and 50‰ for C and N isotope signatures versus NBS 19 calcium carbonate and L-SVEC lithium carbonate and air, respectively. Measurements by GC/IRMS often rely on organic reference materials^{9,34} such as acetanilides and caffeine, which cover slightly smaller $\delta^{13}\text{C}$ and $\delta^{15}\text{N}$ ranges. While a systematic survey of typical $\delta^{13}\text{C}$ and $\delta^{15}\text{N}$ of NACs and RDX is not yet available, the available data suggests that these explosives feature more negative C signatures (down to -50‰) than covered by reference materials that are amenable to the typical gas chromatography conditions applied. Nevertheless, these materials are ideally suited to cross-reference commercially available NACs such as substituted nitrobenzenes across the range of typical $\delta^{13}\text{C}$ and $\delta^{15}\text{N}$ values.

In-house standard materials or mixtures thereof are part of any measurement sequence to compensate for signal drifts and offsets. A representative standard bracketing sequence is made up, for example, of three replicate vials with in-house standard samples followed by three replicate vials of 6–9 sample injections followed by another three replicate vials with control samples. Normalization procedures apply at least two-point calibrations with linear regressions for correct referencing;³⁵ a procedure that is facilitated by spreadsheet templates.³⁶

2.4 Data evaluation

Determination of linear ranges and method quantification limits (MQL) on an isotope ratio mass spectrometer are essential in defining the concentration of analytes required for isotopic analysis. These numbers can vary with instrument type and instrument condition.

MQL are determined using the moving mean procedure proposed by Jochmann et al.³⁷ from the evaluation of a stable isotope signature of a solution containing only the analyte of interest in aqueous or organic solvent at different concentrations. In this approach, the isotope signatures are compared in the sequence of samples from high to low concentrations. The MQL is obtained once the isotope signature of a measurement at lower concentration deviated from the moving mean of all previous data by more than the total uncertainty value. This uncertainty measure is typically better than $\pm 0.5\%$ and $\pm 1.0\%$ for C and N isotope ratio measurements, respectively.³⁸ The lowest concentration in the isotope signature measurement in this range corresponds to the MQL. The concentration range, in which isotope signatures do not change beyond the uncertainty band, is considered the linear range. In this range, isotope ratio measurements are independent of the analyte mass.

Typical MQL determinations are shown in Figures 3 and 4 for $\delta^{15}\text{N}$ and $\delta^{13}\text{C}$ of DNAN determined by SPME arrow as well as for RDX in solutions of ethyl acetate. The two examples for DNAN show the typical observation that MQLs are lower for C than N in most organic compounds due to their larger C than N atom content as well as the higher rare isotope abundance of ^{13}C versus ^{15}N . Note that the moving mean is an operationally defined quality criterion, and those values can deviate from the reference isotope ratio value of the compound determined typically by EA/IRMS. Correction procedures for such offsets are dealt with in the standardization process (described in Section 2.3.5). Note that the peak amplitudes at the MQLs of DNAN measured with SPME-arrow-GC/IRMS were approximately 2-3 times lower (approximately 300 mV) than for most other organic compounds.

For RDX, MQL for $^{15}\text{N}/^{14}\text{N}$ measurements of RDX with the moving mean procedures suggest accurate measurements of 3 nmol N at 130 mV (Figure 4). Dashed lines indicate an uncertainty margin of $\pm 1\%$ relative to the standard value of -4.9% . Carbon isotope analysis of RDX shows that $\delta^{13}\text{C}$ values were highly amplitude dependent between 500 and 4000 mV and complicate accurate $^{13}\text{C}/^{12}\text{C}$ measurements. This effect could be due to interferences of C-containing compounds in the sample as well as in the IRMS that co-elute with RDX in the GC/IRMS system – or it may be an artifact. This result and additional interpretation is discussed in Section 3.3. Even though successful C isotope ratios of RDX are reported (see Section 3.3),^{24,25} this kind of measurement is much more challenging to establish for RDX than for other explosives.

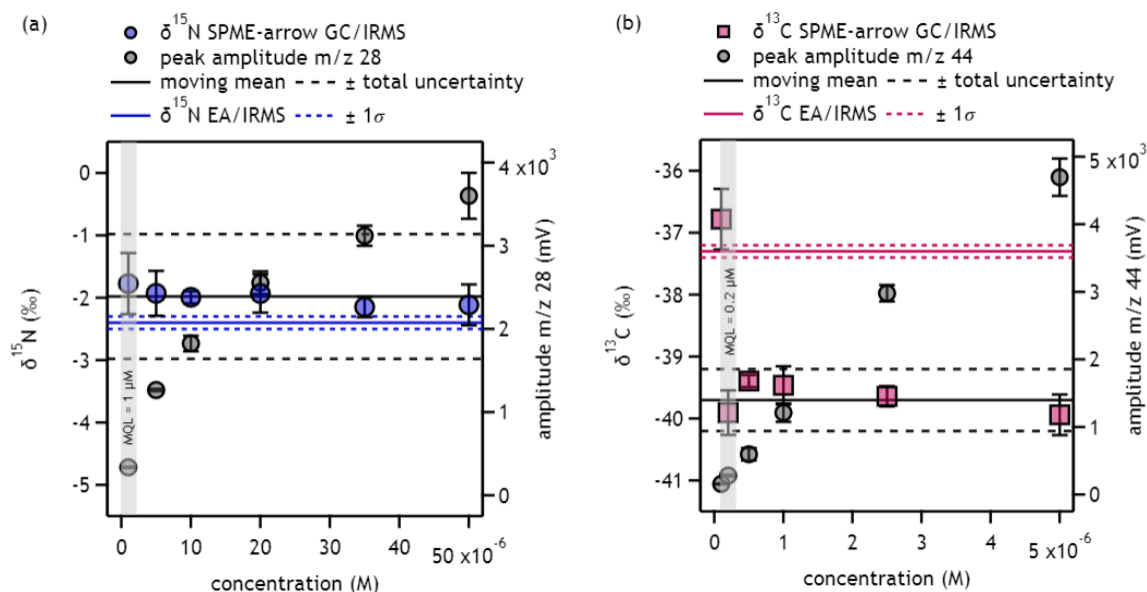


Figure 3. Determination of method quantification limits (MQL) for N and C isotope analysis of DNAN by SPME arrow GC/IRMS. Panels (a) and (b) show data for $\delta^{15}\text{N}$ and $\delta^{13}\text{C}$, respectively. Dashed lines indicate the total uncertainty used for MQL determination as well as one standard deviation of the reference isotope signatures determined by EA/IRMS.

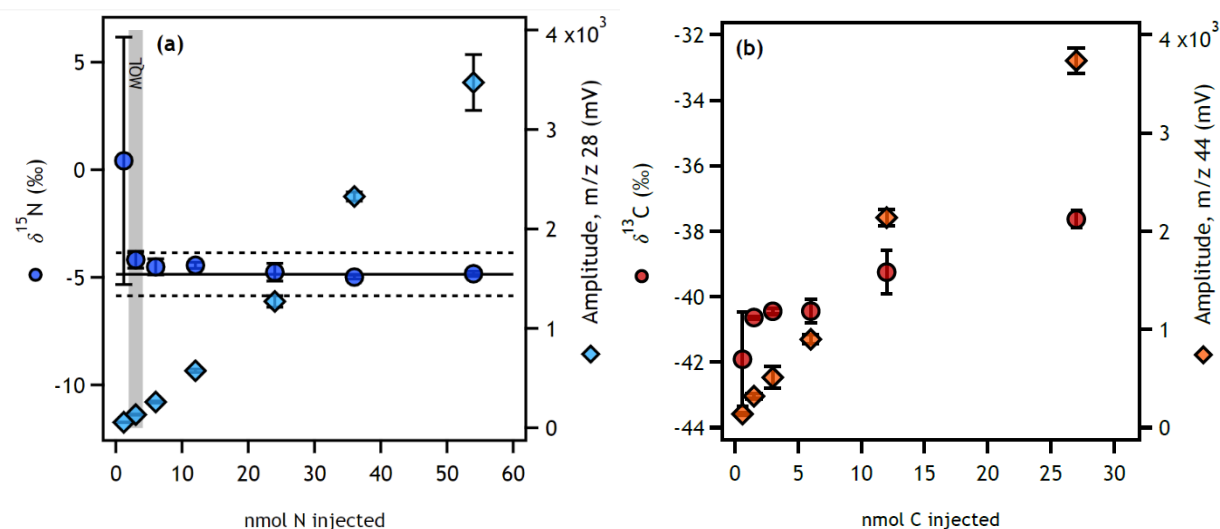


Figure 4. Determination of method quantification limits (MQL) for N and C isotope analysis of RDX by SPME arrow GC/IRMS. Panels (a) and (b) show data for $\delta^{15}\text{N}$ and $\delta^{13}\text{C}$, respectively.

2.5 Data analysis and interpretation

Stable isotope ratios of NACs and RDX can serve two principal purposes: (1) the identification of contamination sources; and (2) the evaluation of transformation processes. Methodologies of source apportionments of explosives, where the isotopic composition of the target analyte is expected to remain constant over time, are not treated here and readers are referred to applications of isotope mixing models.³⁹ Reactive processes, by contrast, cause changes in isotopic composition and this information can be rationalized with different parameters, namely: (1) isotope enrichment factor, ϵ_E ; (2) apparent kinetic isotope effects, $AKIE_E$; as well as (3) the correlation of isotope fractionation of two elements, Λ_{E_1/E_2} (see equations 2 through 7 above).

These parameters are largely determined and used in the following logical sequence. First, ϵ_E -values are derived for a reactive compound and a specific transformation reaction, usually in a laboratory model system. Second, measured ϵ_E values provide the basis for determining $AKIE_E$ s and thus provide information about the type of reaction and kinetics of bond cleavage events. Conversely, it is possible to estimate ϵ_E from $AKIE_E$ s that have been obtained from a structurally related compound in the same reaction. Third, because isotope fractionation is proportional to reaction turnover, ϵ_E values are key to calculate the extent of reaction from measured isotope ratios of the reacting compound, for example, in a contaminated soil or groundwater. Fourth, multi-element ratios of ϵ_E values per compound and reaction are more robust indicators of a reactive process and can be obtained in laboratory experiments from the correlation of $\delta^h E$ values of several elements. The correlation slopes typically denoted as Λ_{E_1/E_2} are compared against correlations of measured isotope fractionation of the same elements, $\Delta E_1/\Delta E_2$ in the system of interest. Finally, several Λ_{E_1/E_2} values for different reactions of the same compound even allow for rationalizing (linear) combinations of reactions leading to a compound's disappearance.⁶ While not accounted for in this discussion, it is important to note that isotopic information is also included in some reactive transport models.^{40,41}

2.5.1 Calculation of isotope enrichment factors

Isotope enrichment factors are typically obtained in laboratory experiments and well-defined field settings from correlating measured isotope ratios with the fraction of remaining reactant:

$$\frac{\delta^h E + 1}{\delta^h E_0 + 1} = \left(\frac{c}{c_0} \right)^{\epsilon_E} = f^{\epsilon_E} \quad (4)$$

or

$$\ln \left(\frac{\delta^h E + 1}{\delta^h E_0 + 1} \right) = \epsilon_E \cdot \ln \left(\frac{c}{c_0} \right) \quad (8)$$

The ϵ_E -values reported in the literature are calculated from both non-linear and linear regression with different recommendations regarding the 'normalization' of the observed isotope fractionation and measured concentrations.^{2,42} This practice makes a precise interpretation of the uncertainties of ϵ_E values difficult, but differences are usually small.⁴³ Note that similar or even higher variations of ϵ_E -values also arise from various other factors such as the control of experimental variables and experiment design and sampling procedures.⁴⁴

2.5.2 Dual element isotope fractionation analysis

Correlation slopes of stable isotope fractionation from different elements in a compound are promising indicators for the type of reaction(s) that lead(s) to contaminant disappearance. However, for their application, two factors need to be accounted for. First, equation 7 is an approximation of the equation below that shows that the dual element isotope fractionation is not a constant.⁴⁵

$$\Lambda_{E_1/E_2} = \frac{f^{\epsilon_{E_1}/1000} - 1}{f^{\epsilon_{E_2}/1000} - 1} \quad (9)$$

where f stands for the fraction of remaining reactant (see spreadsheet template provided by Höhener & Atteia⁴⁵). Deviations become particularly apparent when comparing primary and secondary isotope fractionation as well as for very large isotope fractionation encountered for hydrogen/deuterium.^{12,46} In addition, the currently applied regression methods do not necessarily account for uncertainties in both dimensions of the regression,⁴⁷ an issue that can lead to statistically unprecise regressions and different Λ_{E_1/E_2} values for identical processes. Several authors provide hands-on solutions in terms of spreadsheets and pseudocodes to account for this issue.^{48,49}

3 INTERPRETATION OF STABLE ISOTOPE FRACTIONATION

3.1 Biological, chemical, and photochemical processes

A key to being able to use CSIA to understand reactions processes in field samples is knowing the enrichment factors for the different reactions that are potentially important for the contaminant of interest. These are determined in controlled laboratory experiments. Specific example protocols for hydrolysis, photolysis, abiotic reduction, and anaerobic and aerobic biodegradation experiments are available in the literature.^{6,13,14,21,25,50,51,52} There are, however, key aspects to such experiments that are necessary to consider for measurement of enrichment factors.

Careful design of such experiments includes:

- Isolation of the reaction of interest, with proper controls for hydrolysis/sorption. The experimenter should ensure through careful control of the reaction condition and/or

identification of reaction products that the expected reaction is occurring. Note that if CSIA measurements of reaction products are made, they will reflect the isotope fractionation of the parent compound. That is, if the lighter isotope of the parent reacts more quickly (leading to a heavier isotopic pool of the parent over time), the initial product should be isotopically light, and over time, it reaches the initial isotopic composition of the parent. In heterogeneous systems, mixing must be sufficient to overcome mass transfer limitations, which can mask isotopic fractionation processes.

- Approximately equal spacing of samples over time. At the final time point, 90-95% (at least three half-lives) transformation is ideal, and throughout the reaction, concentrations must be sufficient to allow detection by CSIA. If pre-concentration using SPME or SPE is needed, there must be sufficient sample size/reactor volume to obtain sufficient material without altering the reaction conditions over time. Identically prepared, sacrificial reactors as a function of time are a strategy to allow a sample to be taken to both quantify the amount of the target compound present (which is necessary data) and make CSIA measurements.
- At a minimum, triplicate measurements via CSIA are needed at each time point. This can be three measurements of the sample/extract from a single reactor.
- Understanding of any masking effects, especially in biological systems.¹

Examples of such experiments, and then use of these results in field samples, are presented in the following sections.

3.2 Measurement of Enrichment Factors in Laboratory Experiments

Figure 5 shows the isotope fractionation of nitrogen in RDX under abiotic reducing conditions. For all of the materials, except green rust, aqueous 1 mM Fe(II) was supplied as the reducing agent, and the reaction is mediated by the surface. Because all of the material led to similar isotope fractionation, all of the data were regressed together (individual values for each mineral are available in Tong et al.⁵³) to obtain an ϵ_N value of $-7.4 \pm 0.2\%$. Note that the presence of natural organic matter did not affect the observed fractionation. Experiments at a lower pH value (6.5) led to accumulation of nitroso intermediates that co-eluted with the RDX, complicating the measurement of N and C isotope ratios. As noted above, co-eluting compounds are a common problem in the analysis of C isotope ratios in RDX by GC-IRMS, especially in microbial cultures and field samples.

Figure 6 contains a compilation of ϵ_N values for a variety of RDX transformation processes. The enrichment factor for aerobic biodegradation ($\epsilon_N = \sim -2.5\%$) is distinct from anaerobic biodegradation and abiotic reduction ($\epsilon_N = \sim -7.5\%$). The biological and abiotic reduction processes, however, have similar enrichment factors, because in each case, the same bonds are broken when the nitro group is reduced. Thus, CSIA will reveal that reduction is occurring, but additional information, either geochemical or microbiological, is needed from a field site to assess whether the transformation is biologically or abiotically mediated. The enrichment factor

for hydrolysis is distinct from the other reactions.

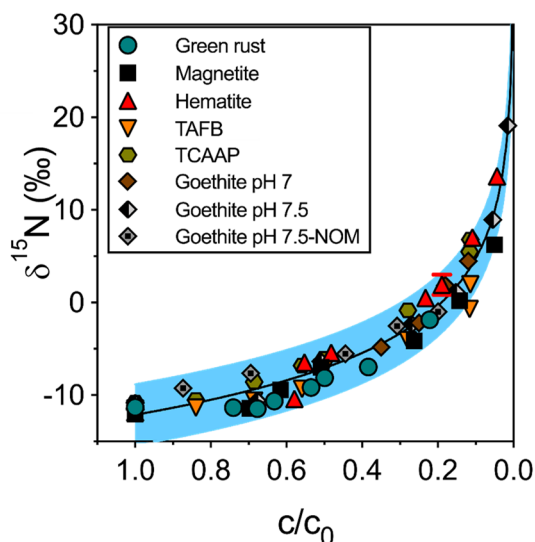


Figure 5. Nitrogen isotope signatures, $\delta^{15}\text{N}$, versus fraction of unreacted RDX (c/c_0) determined in experiments with various Fe(II) containing suspensions. The goethite data represent experiments with Fe(II)/goethite at pH 7.0 and pH 7.5, and Fe(II)/goethite with Elliot Soil Humic Acid at pH 7.5, and all other experiments were carried out at pH 7.5. The curve was fit using the data from each set of conditions to obtain a single ϵ_N value of $-7.4 \pm 0.2\text{‰}$ (individual values in Tong et al.⁵³). The error band shows the 95% confidence interval.

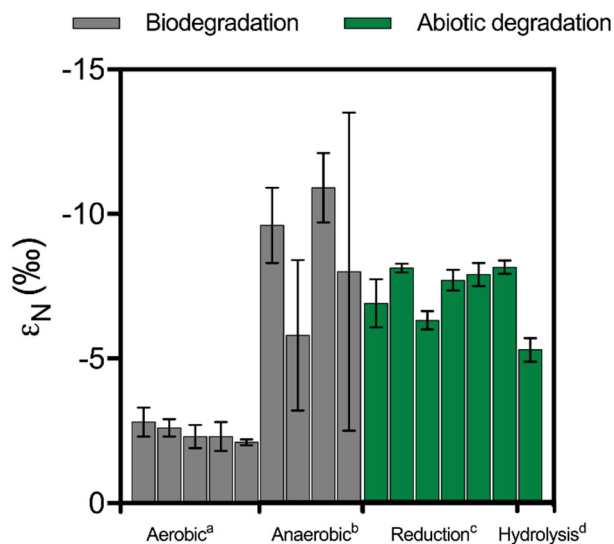
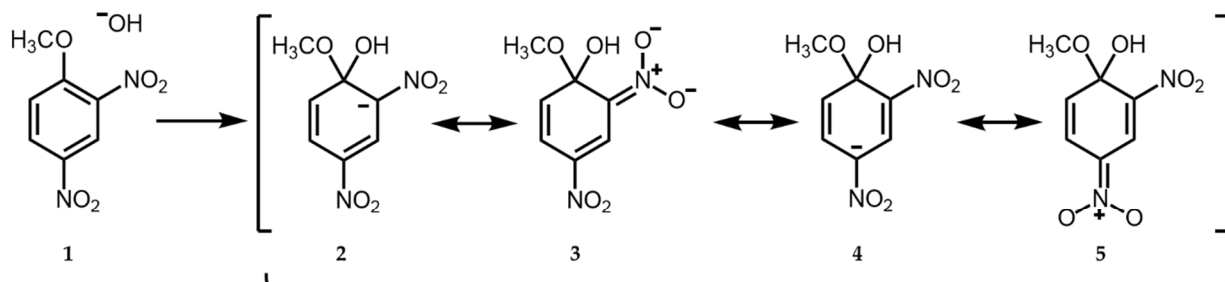


Figure 6. Nitrogen enrichment factors during RDX collected from this study and adapted from previous research under varying experimental conditions. (a) Bernstein et al.;¹⁷ Fuller et al.;²⁵ (b) Fuller et al.;²⁵ (c) this study; (d) Gelman et al.²⁴ Error bars represent the 95% confidence intervals.

3.3 Multi-element isotope fractionation

Additional discrimination among reaction processes is possible if the isotopic fractionation of more than one element is determined. Note that this requires multiple analyses, because isotope ratios of two different elements (e.g., C and N) cannot be measured simultaneously by IRMS. Measurement of multiple isotopes is especially helpful when different processes may lead to similar reaction products. For example, DNAN undergoes a base-catalyzed hydrolysis reaction (Figure 7a). There is also an enzymatic hydrolysis, in which the methoxy C is the reactive site (Figure 7b).

(a) Alkaline hydrolysis



(b) Enzymatic hydrolysis

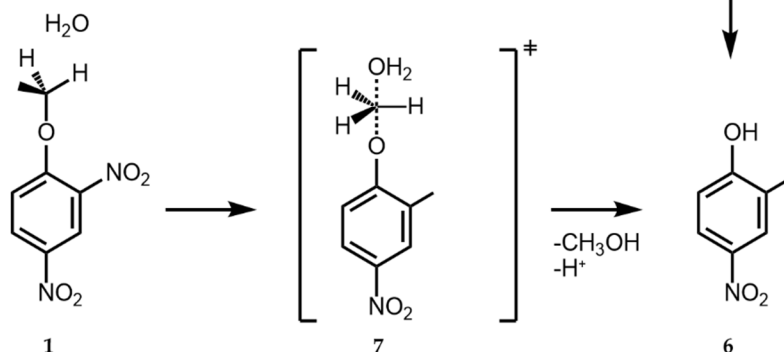


Figure 7. Initial steps for the transformation of 2,4-dinitroanisole (1) by (a) alkaline hydrolysis through nucleophilic aromatic substitution to 2,4-dinitrophenol (6). Compounds 2 to 5 are resonance structures of the Meisenheimer complex intermediates.⁵⁴ (b) Hypothesized enzymatic hydrolysis of DNAN by *Nocardioide*s sp. JS1661 and enzyme assays containing DNAN *O*-demethylase. Compound 7 shows one of several possible transition states for a hydrolytic *O*-demethylation at the aliphatic C atom of the methoxy group.

As shown in Figure 8, the C isotope fractionation for each of these hydrolysis processes is large, and the N isotope fractionation is minimal.

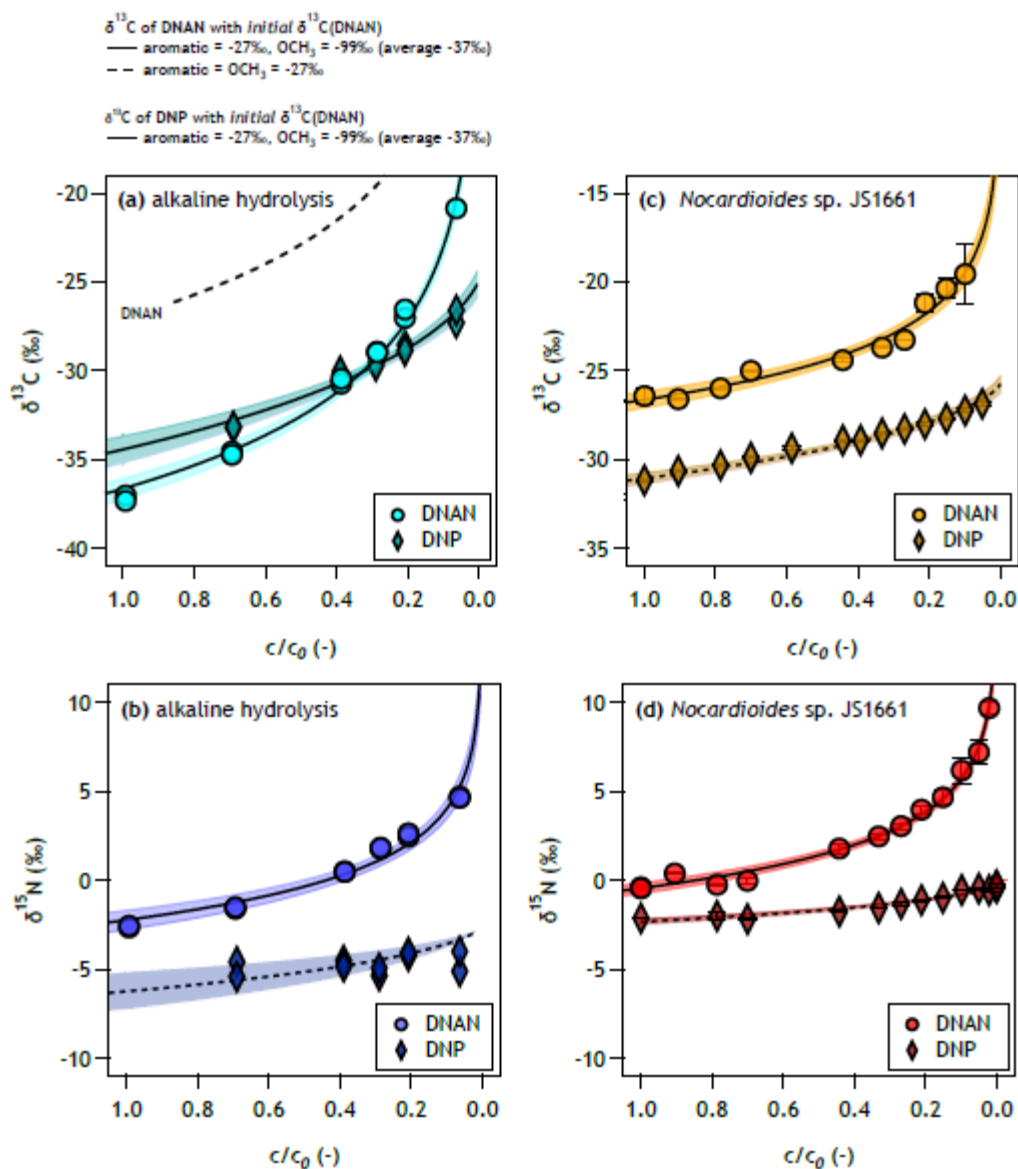


Figure 8. C and N isotope fractionation associated with the transformation of DNAN to DNP by alkaline hydrolysis at pH 12 (panels a and b) and during biodegradation by *Nocardioideis* sp. JS1661 (panels c and d). Panels (a) and (b) show $\delta^{13}\text{C}$ of DNAN and DNP versus fraction of remaining DNAN, c/c_0 ; panels (c) and (d) show the corresponding $\delta^{15}\text{N}$ trends. Lines represent fits of C isotope fractionation (equations 1 and 2) for DNAN and DNP with different assumptions for intramolecular $\delta^{13}\text{C}$ distribution among aromatic and aliphatic C atoms in panel (a). The solid and dotted lines are nonlinear fits to the substrate and product isotope fractionation, respectively. The shaded areas indicate the 95% confidence intervals.

Reduction of DNAN, however, proceeds via nitro group reduction, leading to breakage of an N-O bond:

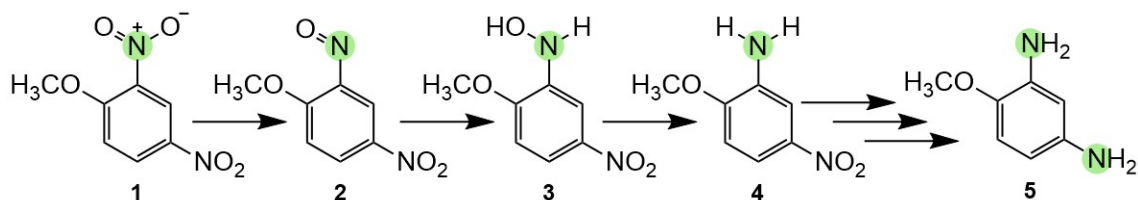


Figure 9. Reduction of DNAN to nitroso (2) and hydroxylamine (3) intermediates. Complete reduction of the first nitro group results in 2-amino-4-nitroanisole (4; 2-ANAN) or 4-amino-2-nitroanisole (4-ANAN) and reduction of both nitro groups results in 2,4-diaminoanisole (DAAN).

Nitro reduction leads to strong fractionation of N, and minimal fractionation of C. Figure 10 demonstrates this for DNAN reaction mediated by Fe(II) in the presence of two synthetic minerals (hematite and magnetite) and two materials collected from contaminated sites, Tinker Air Force Base (the soil contains hematite) and the Twin Cities Army Ammunition Plant (TCAAP; the aquifer material contains magnetite).

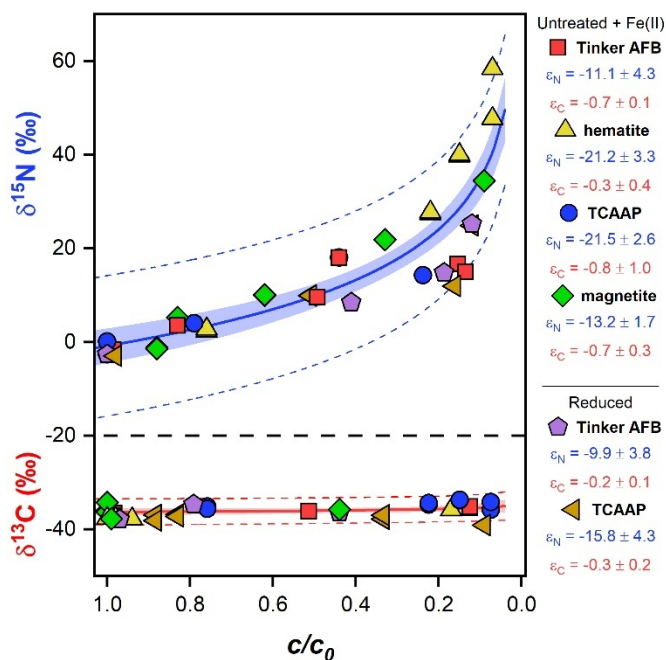


Figure 10. Nitrogen ($\delta^{15}\text{N}$) and carbon ($\delta^{13}\text{C}$) isotope signatures versus fraction of remaining substrate (c/c_0) during DNAN reduction by iron-bearing minerals. Solid lines represent fits from nonlinear regression with shaded portions indicating the 95% confidence intervals. Dashed lines designate 95% prediction intervals. N and C isotope enrichment factors (ϵ_N , ϵ_C) were determined from non-linear regression of the data points for each mineral type. Data are shown for untreated materials in the presence of Fe(II) and dithionite-treated materials.

As demonstrated by the results in Figures 8 and 10, the observed enrichment of N and C is dictated by the bonds broken and the specific energetics involved. The differences in the isotope fractionation for the different reactions are fully apparent by plotting the change in N isotopes versus the change in carbon isotopes (Figure 11). The results from Figures 8 and 10, along with reduction experiments using additional minerals show that the reduction, enzymatic hydrolysis (i.e., biodegradation), and hydrolysis are readily distinguished. Note that if a combination of processes were occurring, the data would fall in between the two lines for the individual processes.

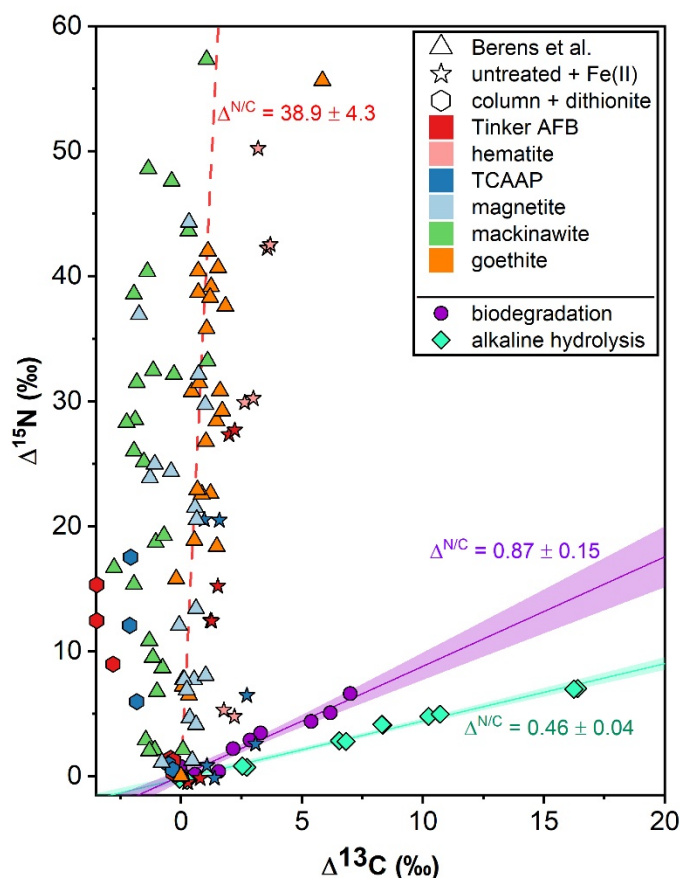


Figure 11. Dual-element (N versus C) isotope analysis to indicate multiple potential DNAN transformation pathways.^{21,52} Data from the present study for abiotic reduction by untreated minerals + Fe(II) (stars) and from columns receiving in situ chemical reduction (ISCR) (hexagons) are shown. The dotted line represents the fit from linear regression by the York method as described by Ojeda et al.⁴⁸ The isotope fractionation observed during biodegradation (circles) and alkaline hydrolysis (diamonds) are provided for reference. Shaded portions represent the 95% confidence intervals from nonlinear regression analysis.

An evaluation of $\delta^{13}\text{C}$ values of RDX standards measured as part of the standard bracketing procedures suggest that the observed amplitude dependence of $\delta^{13}\text{C}$ in Figure 4 could have been an artifact. Figure 12 shows the $\delta^{13}\text{C}$ of 36 RDX standards injections (blue symbols) that accompanied the C isotope analysis of RDX reduction experiments in suspensions of Fe(II)/hematite and green rust. These data align well with the $\delta^{13}\text{C}$ of the highest peak amplitude of the C isotope ratio linearity test shown in Figure 4 (data from this figure is reproduced in Figure 12) and suggested a $\delta^{13}\text{C}$ of RDX of $-37.4 \pm 0.2\text{‰}$. The data also suggest that reproducible C isotope ratios within the amplitude range between 1000 and 4000 mV is feasible (grey shaded box). Figure 12 also shows $\delta^{13}\text{C}$ and signal amplitudes of RDX measurements from abiotic reduction experiments. All of these fall within the amplitude range of C isotope ratio measurements of RDX standards except for three samples where RDX was above 4000 mV. Note that these high amplitudes are from experimental samples with low aqueous RDX concentrations where a larger fraction of the solvent was evaporated to obtain measurable RDX quantities. The team did not find evidence that the evaporation step caused C (or N) isotope fractionation.

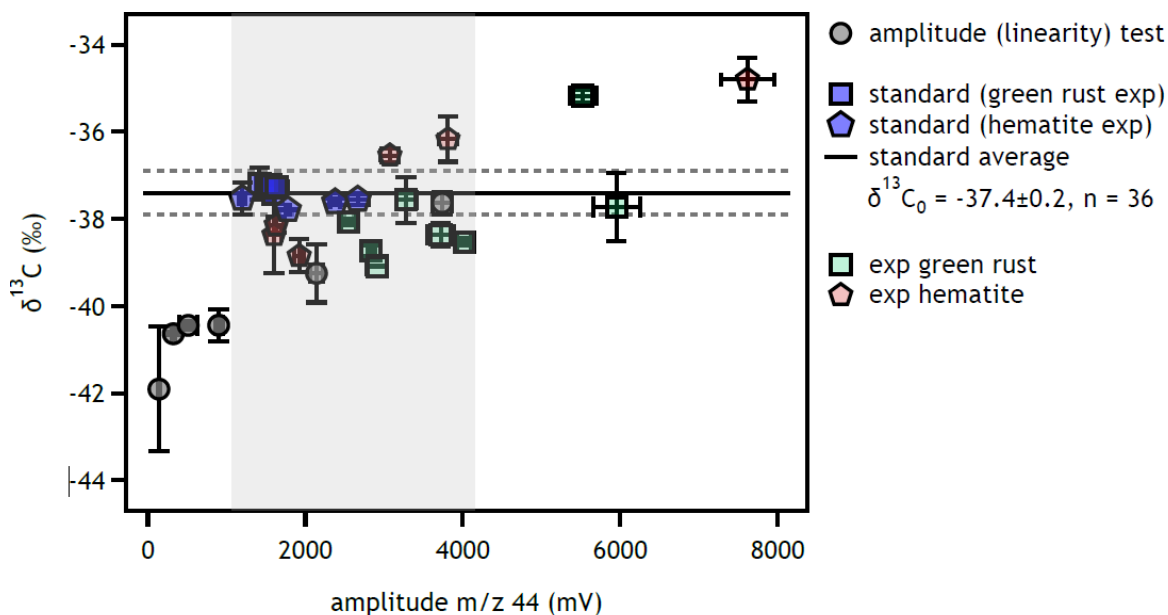


Figure 12. $\delta^{13}\text{C}$ of RDX versus signal amplitude for RDX standard injections performed during the analysis of RDX samples from RDX reduction experiments in Fe(II)/hematite and green rust suspensions (red/green symbols). The grey area delineates the amplitude range of constant $\delta^{13}\text{C}$ for RDX standard measurements.

The extent of C isotope fractionation in RDX reduction experiments with suspensions of green rust and Fe(II)/hematite is shown in Figure 13. Note that C isotope analysis in other experiments was not possible due to the presence of an intermediate substance peak that co-eluted with RDX.

The range of $\delta^{13}\text{C}$ was moderately small and within less than 4‰ and C isotope enrichment factors, ϵ_{C} , obtained from non-linear regression amounted to $-2.6 \pm 1.0\text{‰}$ and $-2.0 \pm 0.5\text{‰}$ ($\pm 95\%$ confidence intervals) for green rust and Fe(II)/hematite experiments, respectively. These ϵ_{C} -values were obtained by including C isotope ratio measurements at peak amplitudes exceeding 4000 mV (grey symbols in Figure 13). Excluding these data points led to slightly smaller ϵ_{C} -values of $-1.5 \pm 1.1\text{‰}$ and $-1.8 \pm 0.1\text{‰}$.

Despite some uncertainty associated with C isotope ratios measurements, the data suggest RDX reduction is accompanied by C isotope fractionation that corresponds to a secondary ^{13}C AKIEs of approximately 1.002 ± 0.001 given that no bonds to C atoms are directly participating in the initial reduction of the NO_2 moiety of the nitramines. This ^{13}C AKIE value is also in agreement with secondary C isotope fractionation of aromatic C atoms during abiotic reduction of NACs. Secondary C isotope fractionation has also been reported for aerobic denitration of RDX for which a rate-limiting N–N bond cleavage is hypothesized. This reaction was accompanied by similarly small ϵ_{C} -values of $-0.9 \pm 0.8\text{‰}$ ⁵⁵ supporting the team's interpretation of a secondary ^{13}C AKIE.

The team also correlated the C versus N isotope fractionation to determine $\Delta_{\text{N/C}}$ values that might be characteristic for abiotic RDX reduction by Fe minerals. Figure 14 shows that both experiments gave rise to similar numbers: 2.6 ± 0.7 (green rust) and 5.4 ± 2.6 (Fe(II)/hematite) within uncertainty. The moderately large slopes reflect the fact that the large ^{15}N -KIEs of RDX are strongly diluted by the 6 N atoms of RDX, which leads to a substantially lower slope than that for DNAN (Figure 11). Due to the small measurement uncertainties for both C and N isotope signatures, linear regressions following the York method did not lead to mathematically different results (2.7 ± 0.1 and 5.7 ± 0.7 for green rust and Fe(II)/hematite, respectively).

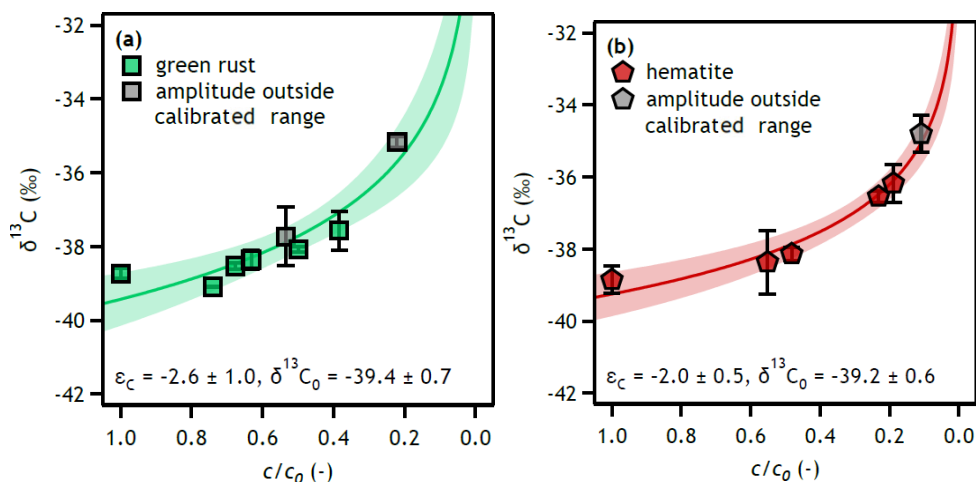


Figure 13. Carbon isotope fractionation of RDX in reduction experiments in suspensions of green rust (panel a) and Fe(II)/hematite (panel b). ϵ_{C} - values and initial RDX C isotope

signatures ($\delta^{13}\text{C}_0$) were obtained from non-linear regression. Parameter uncertainties and shaded areas represent 95% confidence intervals.

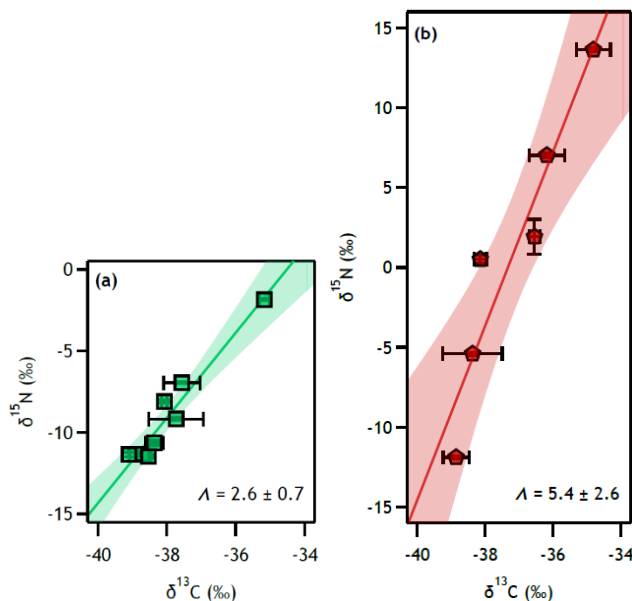


Figure 14. Correlation of C and N isotope fractionation of RDX reduction in suspensions of green rust (panel a) and Fe(II)/hematite (panel b) Error bars are standard deviations of triplicate C and N isotope ratio measurements, shaded areas indicate 95% confidence intervals of the linear regression.

For many potential reaction processes of nitro compounds, enrichment factors have been measured allowing $\Lambda_{\text{N/C}}$ values to be determined (see Table 1 for a summary and Appendix A for a list of parameters for NACs and RDX). These have largely been validated across multiple studies.

Table 1. Representative enrichment factors and kinetic isotope effects for explosives.^{6,52,53,56–61} A complete listing for various NACs and explosives is given in Appendix A.

NAC	ϵ_{N} (‰)	^{15}N -AKIE	ϵ_{C} (‰)	^{13}C -AKIE	reaction
DNAN	-15	1.031	-0.67	1.0010	abiotic reduction
	-2.8	1.0028	-4.2	1.0303	enzymatic hydrolysis
	+12.3	ND	-3.3	ND	direct photolysis
RDX	-7.4	1.045	-2.3	1.002	abiotic reduction
	-3.4	ND	-3.2	ND	aerobic biodegradation
TNT	-8.6	1.026	ND	ND	abiotic reduction
2,4-DNT	-13	1.0273	-0.59	1.0034	reduction
	-1.2	1.0024	-0.5	1.0035	aerobic biodegradation

ND = no data

In contrast to the normal isotope fractionation patterns described above for nitro reduction and alkaline hydrolysis of DNAN, inverse isotope fractionations of both C and N have been observed

in photolytic degradation driven by UV-A and UV-C irradiation of DNAN in aqueous solution.⁶⁰ In this study, photolysis experiments were performed using a Rayonet® RPR-200 photoreactor. Interestingly, under UV-A (~350 nm) irradiation, normal C fractionation ($\epsilon_C = -3.34 \text{ ‰}$) and inverse N fractionation ($\epsilon_N = +12.3 \text{ ‰}$) were measured, whereas the opposite sense of fractionation was measured under UV-C (~250 nm) irradiation ($\epsilon_C = +1.45 \text{ ‰}$, $\epsilon_N = -3.79 \text{ ‰}$). Both sets of DNAN photolysis data, however, yield negative $\Delta_{N/C}$ correlation slopes on a $\Delta^{15}\text{N}$ versus $\Delta^{13}\text{C}$ diagram (Figure 15), indicating that UV-induced isotope effects (caused by exposure to sunlight or by UV applied during wastewater treatment processes) may be easily discerned from other chemical or biological isotope effects (i.e., compare Figures 11 and 15).

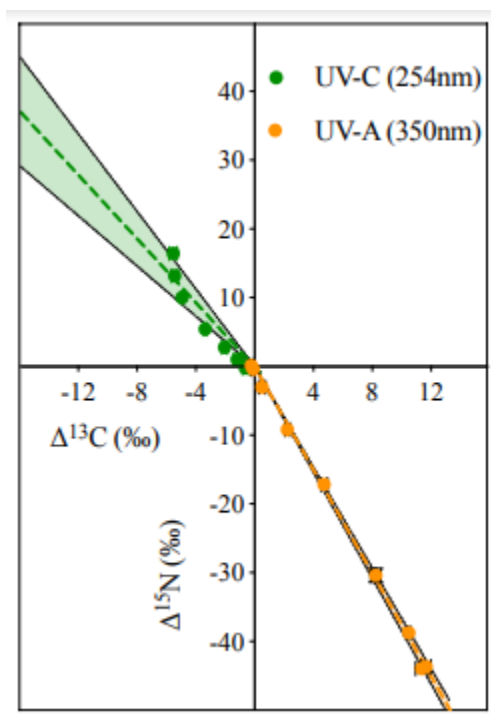


Figure 15. $\Delta\delta^{13}\text{C}$ (‰) and $\Delta\delta^{15}\text{N}$ (‰) in DNAN during photolysis under UV-A (~350 nm) and UV-C (~250 nm) irradiation. Initial DNAN isotope composition: $\delta^{13}\text{C} = -37.2 \text{ ‰}$ and $\delta^{15}\text{N} = -2.5 \text{ ‰}$. Dashed gray lines are 95% confidence intervals of the linear regressions (from ref⁶⁰).

3.4 Application of CSIA to field samples: Case Studies

3.4.1 Iowa Army Ammunition Plant (IAAAP)

CSIA was applied to evaluate RDX transformation in seven monitoring wells along Line 800 of a subsurface plume at the IAAAP (Figure 16). Approximately 3–4 L of groundwater from each well was collected into clean one-gallon glass jugs, filtered through a pre-combusted 0.45 μm glass fiber filter (MilliporeSigma, GF/F), and stored in a cold room (4 °C) until further analysis. The filtered samples were enriched for RDX content using SPE.

Concentrations of RDX ranged from $<0.01 \mu\text{M}$ to $29.3 \mu\text{M}$ and decreased radially from sampling point G-20, where the highest value was measured. Samples from only four monitoring wells exceeded concentrations of $0.1 \mu\text{M}$ and were suitable for N isotope ratio measurements of RDX. These wells also had low dissolved oxygen, consistent with reducing conditions (Table 2).

The G-20 sample was assumed as the reference point for CSIA of RDX because of its upstream location along the hydrologic gradient.^{62,63} It is in close proximity to the source of the plume⁶⁴ and coincides with the highest aqueous RDX concentration and smallest $\delta^{15}\text{N}$ ($+0.66\%$). This operational $\delta^{15}\text{N}_0$ is within the range of data from published analyses of manufactured RDX,

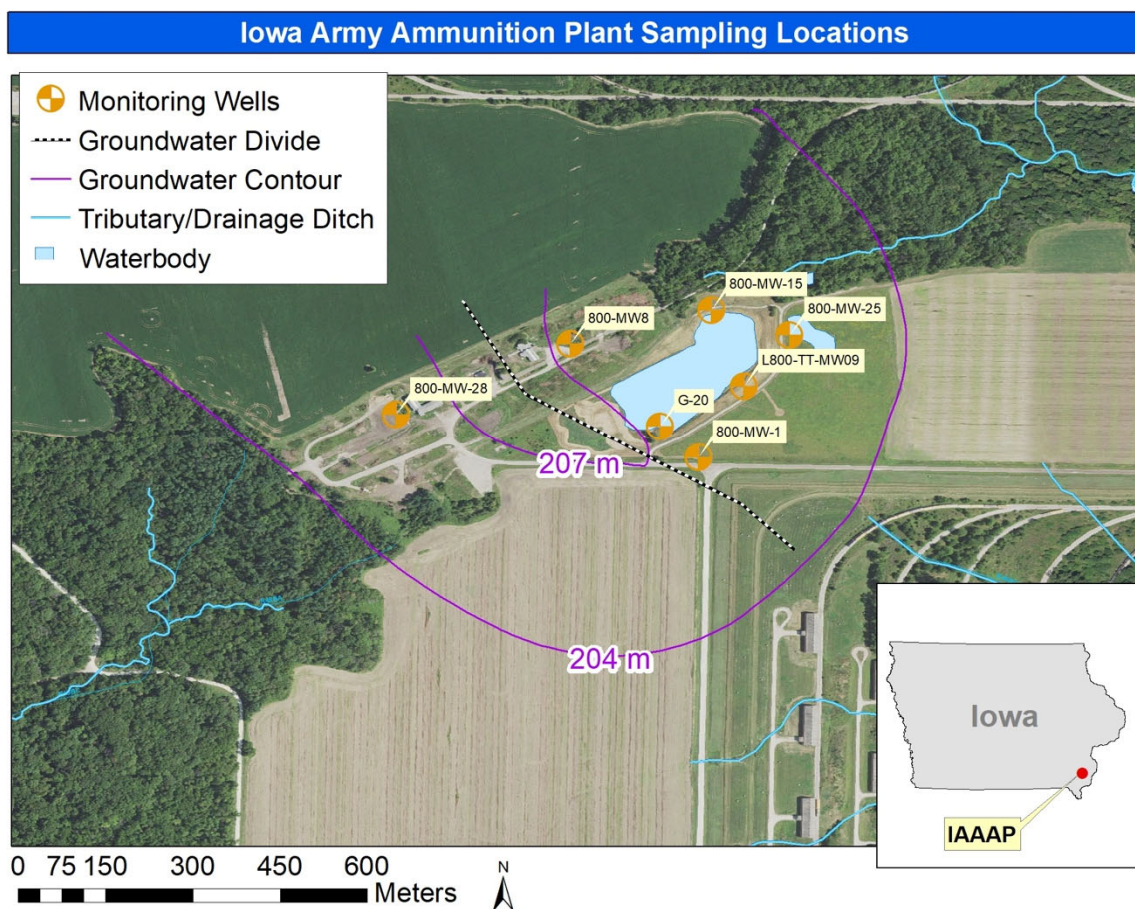


Figure 16. Local map of IAAAP monitoring wells sampled RDX analysis. Ground water contours are labelled with 207 m and 204 m. Lines without labels are tributaries and drainages ditches.

which vary from -17% to $+8.5\%$ depending on synthesis method and raw materials.²⁶ The $\delta^{15}\text{N}$ value of G-20 could reflect some degradation of RDX given the historic concentrations of RDX ($>50 \mu\text{M}$) reported for 1990-2000.^{26,64} Figures 17a and b show that decreasing RDX concentrations in the sampling wells considered here also correspond with $\delta^{15}\text{N}$ values

increasing by ~15‰. The presence of typical RDX reduction products, MNX, DNX, TNX in concentrations <1.0 μM (Figure 17c) supported the assumption of reductive RDX transformation in the subsurface.

Based on the detection of RDX reduction products typically associated with reduction (the process could be biological or abiotic, as the isotope analysis cannot differentiate between the two – see Figure 6), the team evaluated the extent of RDX transformation relative to the $\delta^{15}\text{N}$ values measured from sampling well G-20 and the average isotope enrichment factor obtained from the batch experiments ($\epsilon_{\text{N}} = -7.4\text{‰}$). Figure 17a shows that calculated RDX concentrations after abiotic reduction with this ϵ_{N} -value range between 5 and 15 μM , compared to measured concentrations of 0.1, 0.8, and 3 μM . These predicted concentrations correspond to an extent of reductive transformation of 54% to 85%. If reduction was the predominant mode of RDX transformation, our data would imply that the measured, lower concentrations were also the consequence of other non-isotope fractionating processes (e.g., sorption, dilution, volatilization). Given that RDX sorption to the solid matrix is likely negligible and that RDX is largely non-volatile, the team hypothesizes that the observed decreases in concentration, beyond those predicted by CSIA, were due to dilution. Overall, these data demonstrate the utility of CSIA in demonstrating that transformation has taken place and in bounding the extent of decrease in concentration due to reaction versus dilution/sorption. The results also show the utility of additional data (redox conditions, detection of reaction intermediates) in identification of the reaction process occurring.

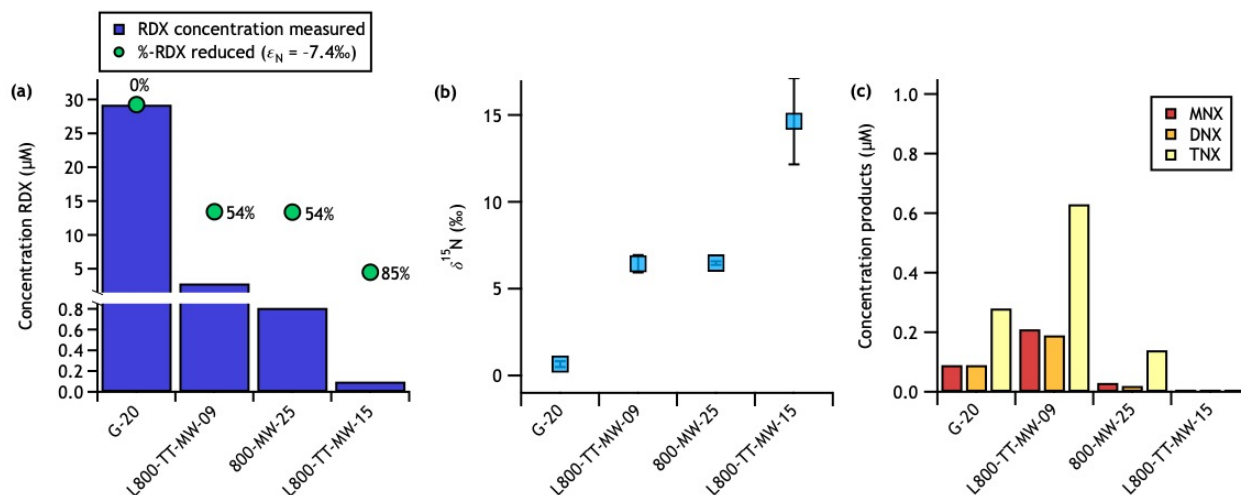


Figure 17. Evaluation of RDX concentrations and $\delta^{15}\text{N}$ values with regard to reductive transformation in monitoring wells along Line 800 at IAAAP (see map Figure 16). The samples are sorted according to increasing distance from the operationally defined contamination source, well G-20. (a) Aqueous concentrations of RDX at different sampling locations including calculated extent of RDX reduction (equation 5) based on the ϵ_{N} -value obtained in laboratory batch experiments with Fe-minerals. (b) $\delta^{15}\text{N}$ values of RDX at different sampling locations. (c) Concentrations of partially reduced RDX reduction products.

Table 2. Chemical data from the collected groundwater samples from the Iowa Army Ammunition Plant.

Well	Sampling Date	RDX (μM)	RDX $\delta^{15}\text{N}$ (‰)	MNX (μM)	DNX (μM)	TNX (μM)	Depth to water (ft bgs)	Conductivity ($\mu\text{S}/\text{cm}$)	DO (mg/L)	ORP (mV)
G-20	2018-8-28	29.3	0.7 ± 0.2	0.09	0.09	0.27	13.09	912	0.42	-12.8
L800-TT-MW-09	2018-8-28	2.84	6.4 ± 0.5	0.21	0.19	0.63	9.23	650	0.15	141
800-MW-25	2018-8-18	0.8	6.5 ± 0.1	0.03	0.02	0.14	10.30	540	0.28	176
L800-TT-MW15	2018-8-28	0.10	14.6 ± 2.5	3.3×10^{-3}	5.8×10^{-4}	1.6×10^{-3}	17.39	2310	2.17	232
800-MW-28 ^a	2018-8-27	0.005	-	4.0×10^{-3}	8.9×10^{-4}	1.1×10^{-3}	ND	ND	ND	ND
800-MW-1 ^a	2018-8-18	0.08	-	1.6×10^{-3}	4.4×10^{-4}	4.5×10^{-3}	ND	ND	ND	ND
800-MW-8 ^a	2018-8-19	0.01	-	7.3×10^{-4}	5.3×10^{-4}	1.1×10^{-3}	ND	ND	ND	ND
^a RDX concentration too low to measure $\delta^{15}\text{N}$ values. ND = no data										

3.4.2 Pantex Plant

A recent study of the natural attenuation of RDX in groundwater at the U. S. Department of Energy's Pantex plant in the Texas panhandle combined the results of GC/IRMS analyses of N isotope ratios in RDX with metagenomics and proteomics data, in addition to chemical analyses of RDX and its degradation products.¹⁵ Microorganisms present in raw groundwater samples were cultured in sterile basal salts medium amended with RDX, sodium succinate, and glucose to confirm activity.

Groundwater samples were collected from 24 wells screened in a perched aquifer 70-90 m below ground surface using a low-flow pump and standard procedures to ensure well stabilization based on field parameters of temperature, pH, dissolved oxygen, and oxidation-reduction potential. A map of the study site is shown in Figure 18. After sampling for all other analyses, pumping rate was increased to increase sample biomass for metagenomics and proteomics analyses. Samples for CSIA were collected in 1000-mL amber high density polyethylene bottles, acidified with HCl, and packed in a cooler with ice for shipment to the laboratory where they were chilled to 4 °C until RDX was extracted and purified by treatments with SPE.

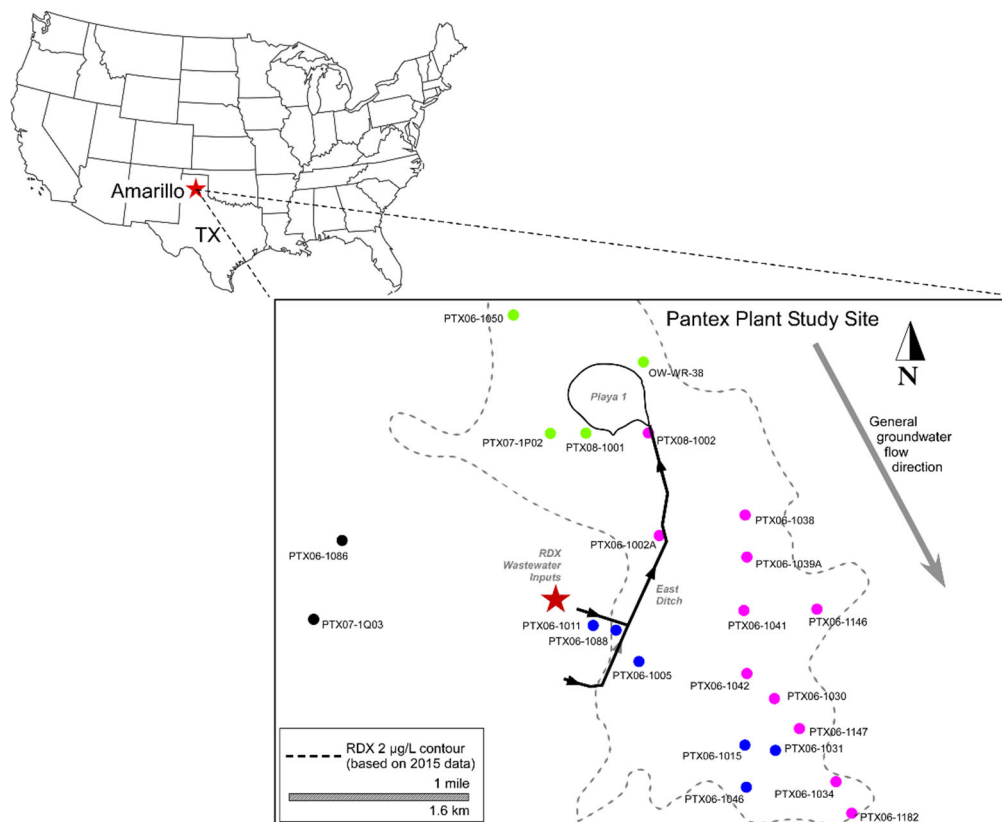


Figure 18. Map of the study site, indicating key topographic features and wells sampled. Colors designate three transects. The dashed line represents the 2 µg/L RDX contour in 2015 (from ref ¹⁵).

Historical activities at the Pantex plant involved formulation of explosive components used in the nuclear arsenal, primarily mixtures of TNT, RDX, HMX. From 1952 to 1985, large volumes of wastewater (estimated 224,000 to 314,000 gallons per day) containing RDX and other explosive compounds flowed out of Zone 12 into the unlined East Ditch, discharging via a surface waste trench into a natural basin designated as Playa 1 (Figure 18). Starting in 1985 and continuing until 1999, treated wastewater was discharged, and all discharges were stopped in 1999. Groundwater flow direction within the perched aquifer is generally toward the southeast. Relatively high concentrations of RDX (up to 1669 $\mu\text{g/L}$) and 4-nitro-2,4-diazabutanal (NDAB; up to 208 $\mu\text{g/L}$) were measured in most of the groundwater samples (Figure 19; Table 3). NDAB is produced from RDX by aerobic biodegradation and alkaline hydrolysis. Appreciable concentrations of nitroso-containing metabolites produced by anaerobic and abiotic nitro reduction of RDX as well as other explosives (HMX, nitrobenzenes, and nitrotoluenes) were also measured in some wells (Figure 19). Concentrations of RDX and RDX breakdown products appear to be correlated in the study area and generally increased from north to south and from west to east. The highest concentrations are found to the east and southeast from the presumed source locations along the East Ditch and Playa 1. Lower concentrations were observed near the source locations, likely due to reduced contaminant loading of infiltrating water due to treatment or elimination of wastewater flows. The distribution of RDX and RDX degradation products aligns with the general groundwater flow direction and suggests common transport of RDX and its breakdown products in the plume.

Values of $\delta^{15}\text{N}$ in RDX ranged from -5.4 to $+9.3\text{‰}$ (Figure 20), with higher values generally occurring near the presumed source region where RDX concentrations are lowest, and lower values generally occurring from 1 to 5 km downgradient of the source region where RDX concentrations are highest. Interpretations of this pattern are complicated by the possibility that several different degradation processes having different ϵ_{N} values may have operated at the site, and there may have been different initial $\delta^{15}\text{N}$ values of RDX used at the site over its decades-long history. However, extents of degradation obtained by assuming a source of RDX having the isotopic composition observed in well PTX06-1005 (-4.1‰) and different characteristic ϵ_{N} values (e.g., for aerobic biodegradation, anaerobic biodegradation, or alkaline hydrolysis) yielded reasonable agreement with the chemical, metagenomic and proteomic evidence for both aerobic and anaerobic degradation, as well as with the expected extent of abiotic hydrolysis that may have occurred over the 33 – 66 years elapsed between RDX discharge and sampling. The 16S metagenomic sequencing data from the Pantex site demonstrated that a diversity of RDX degrading bacteria were present, and proteomic data suggested that several RDX degrading bacterial species were alive and active. Groundwater enrichment cultures confirmed the potential of the groundwater microbial community to aerobically degrade RDX and produce NDAB upon addition of labile carbon.

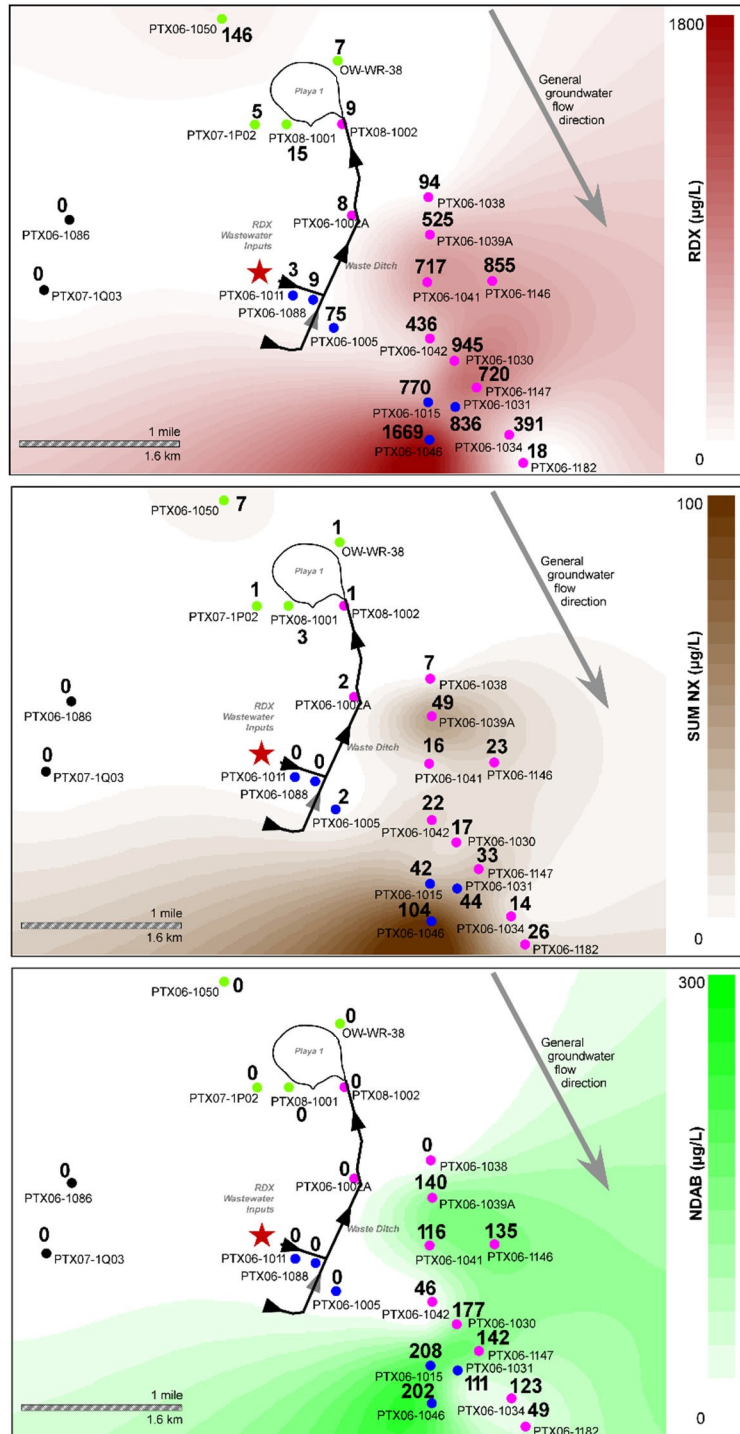


Figure 19. Detected concentrations of explosives and breakdown products in groundwater at the Pantex study site. A) RDX; B) Sum of nitroso-containing RDX breakdown products; C) NDAB (from ref ¹⁵).

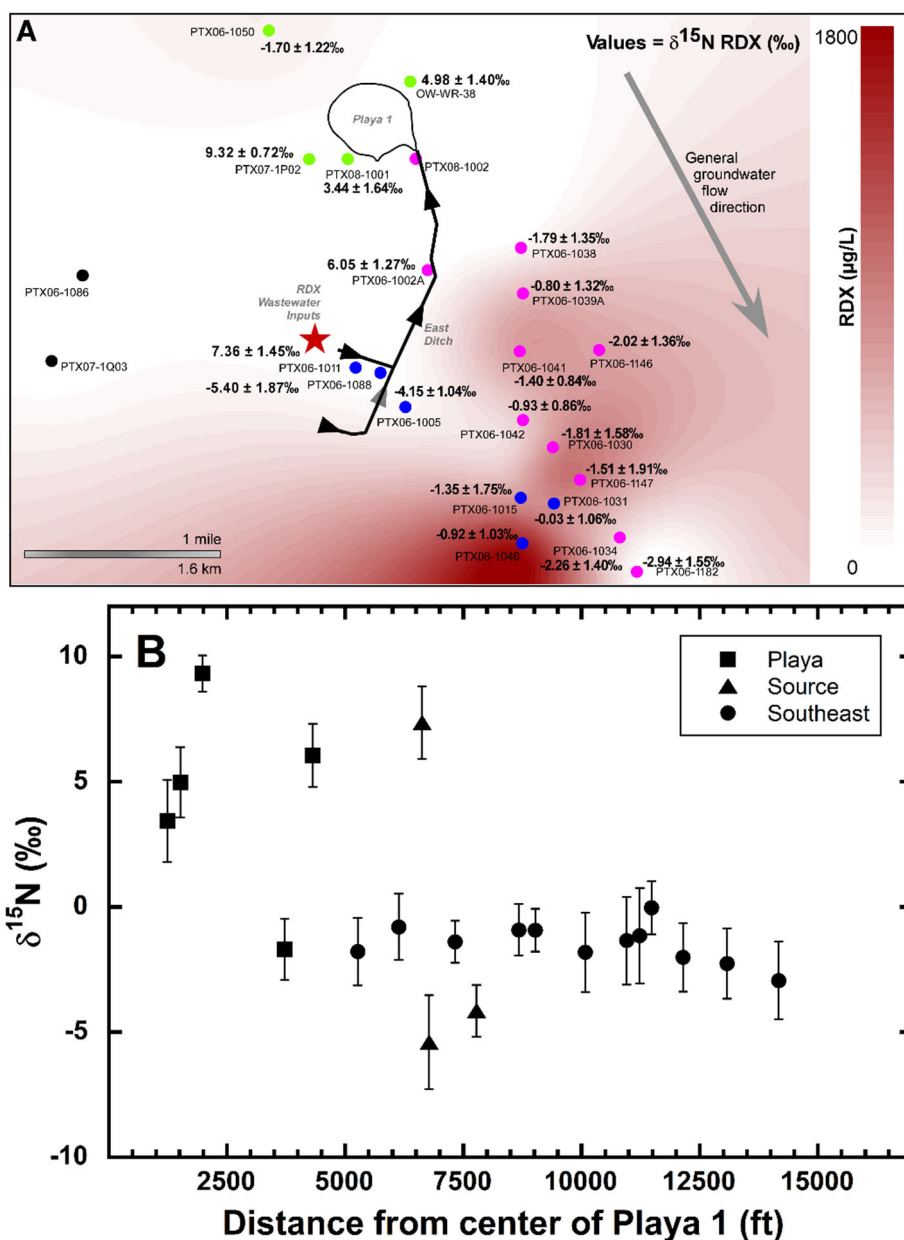


Figure 20. A) Summary of RDX $\delta^{15}\text{N}$ results. The RDX concentration contour surface is shown for reference. B) $\delta^{15}\text{N}$ values of RDX as a function of the distance from the center of Playa 1. Symbols represent wells in immediate vicinity of Playa 1 (squares), near the location of RDX source release into the ditch (triangles), or in the southeastern region of the current plume (circles) (from ref 15).

Table 3. Summary of detections of RDX, RDX breakdown products, $\delta^{15}\text{N}$ values of RDX and other explosives in groundwater collected for the Pantex study. ND = Not detected or no data. Data is from ref. ¹⁵.

WELL ID	NDAB $\mu\text{g/L}$ 20	MNX $\mu\text{g/L}$ 0.025	DNX $\mu\text{g/L}$ 0.025	TNX $\mu\text{g/L}$ 0.025	SUM NX $\mu\text{g/L}$	HMX $\mu\text{g/L}$ 0.01	RDX $\mu\text{g/L}$ 0.01	$\delta^{15}\text{N}$ in RDX (‰)	\pm	n
PTX06-1011	<20	<0.025	<0.025	0.1	0.1	<0.01	3	7.36	1.45	2
PTX06-1088	<20	<0.025	<0.025	0.3	0.3	1.4	9	-5.40	1.87	4
PTX06-1005	<20	<0.025	<0.025	2.3	2.3	50.0	75	-4.15	1.04	6
PTX06-1015	208	<0.025	<0.025	42.4	42.4	94.1	770	-1.35	1.75	20
PTX06-1031	111	<0.025	<0.025	43.9	43.9	53.5	836	-0.03	1.06	9
PTX06-1046	202	<0.025	<0.025	104.3	104.3	236.6	1669	-0.92	1.03	11
PTX06-1050	<20	0.8	<0.025	6.3	7.1	9.1	146	-1.70	1.22	11
OW-WR-38	<20	<0.025	0.1	1.1	1.2	4.2	7	4.98	1.40	9
PTX07-1P02	<20	<0.025	<0.025	0.8	0.8	0.4	5	9.32	0.72	9
PTX08-1001	<20	<0.025	1.0	1.8	2.7	1.2	15	3.44	1.64	12
PTX08-1002	<20	<0.025	<0.025	1.3	1.3	5.5	9	ND	ND	ND
PTX06-1038	<20	0.7	<0.025	6.6	7.4	43.6	94	-1.79	1.35	12
PTX06-1002A	<20	0.2	0.5	1.5	2.2	0.9	8	6.05	1.27	8
PTX06-1039A	140	5.7	6.2	37.4	49.3	111.8	525	-0.80	1.32	11
PTX06-1041	116	3.1	<0.025	12.9	16.0	54.7	717	-1.40	0.84	25
PTX06-1146	135	7.3	<0.025	15.3	22.6	43.1	855	-2.02	1.36	8
PTX06-1042	46	5.4	5.1	11.9	22.4	45.9	436	-0.93	0.86	14
PTX06-1030	177	6.9	<0.025	10.4	17.3	100.4	945	-1.81	1.58	12
PTX06-1147	142	5.1	<0.025	28.2	33.3	117.8	720	-1.15	1.91	11
PTX06-1034	123	2.3	<0.025	13.5	15.8	67.9	391	-2.26	1.40	20
PTX06-1182	49	3.9	13.7	8.5	26.1	28.1	18	-2.94	1.55	5
PTX07-1Q03	<20	<0.025	<0.025	<0.025	<0.025	<0.01	<0.01	ND	ND	ND
PTX06-1086	<20	<0.025	<0.025	<0.025	<0.025	<0.01	<0.01	ND	ND	ND

3.5 Using CSIA Results to Aid in Interpretation of Field Data

Measuring the fractionation of C and N isotopes along a groundwater flowpath provides valuable information that aids in assessment of the extent of, and process responsible for, contaminant degradation. That said, full assessments require additional data and careful interpretations must be carefully made.

Figure 21 provides guidance for interpreting results. For identification of the reaction process (Figure 21 top), site characterization is needed, including redox conditions and geochemical parameters of the groundwater (e.g., dissolved oxygen, presence of ferrous iron). As shown for IAAAP, low dissolved oxygen was an indicator of reducing conditions. Assessment of the site microbiology via molecular techniques could also be valuable. Measurement of concentration trends along the flow gradient(s) for both the nitro compound and potential reaction products also provides indications of which reaction processes are occurring, as seen for both the IAAAP and Pantex sites.

Using the changes in concentrations of the substrate and identified products and/or the site conditions, possible reaction pathways are assessed using Figure 1. Reductive transformations (green labels in Figure 1), whether biological or abiotic, will give different isotope fractionations than those for oxidative (red) or hydrolytic (blue) reactions. Hydrolytic reactions may occur under both oxidative and reductive conditions. It may be that concentrations of the parent decrease, products are not seen, and in this case, the site conditions indicate possible processes, but it is harder to draw a definitive conclusion.

Once possible reactions based on site conditions are assessed, the CSIA results can be used to confirm the transformation process and estimate the extent of transformation (Figure 21 bottom). For nitro compounds, large isotopic fractionation of N is indicative of a reductive process. Ideally, both N and C isotopes are measured allowing use of the $\Delta^{15}\text{N}$ vs $\Delta^{13}\text{C}$ plot, where slopes $\gg 1$ are consistent with reductive processes and slopes of approximately 1 or below < 1 suggest processes that are non-reductive (see Figure 11). For the reductive processes of interest in this document, the ϵ_{N} and/or ϵ_{C} values measured in laboratory experiments with model, and (if possible) site, materials are then used to estimate the extent of transformation using equation 5. For a reductive process, only ϵ_{N} is used, for there is little or no C isotope fractionation. As shown for the IAAAP site, the extent of transformation predicted was less than the change in concentration observed. This indicates that other processes that do not fractionate N isotopes are partially responsible for the concentration decrease. While other reactive processes that degrade the contaminant fractionate N isotopes to much lesser extent than reductive processes, the conservative assumption is that these concentration decreases are due to non-reactive processes, such as dilution or sorption. Similar calculations can be performed for oxidative/hydrolytic transformations using literature values of ϵ_{N} and/or ϵ_{C} for the appropriate reaction process.

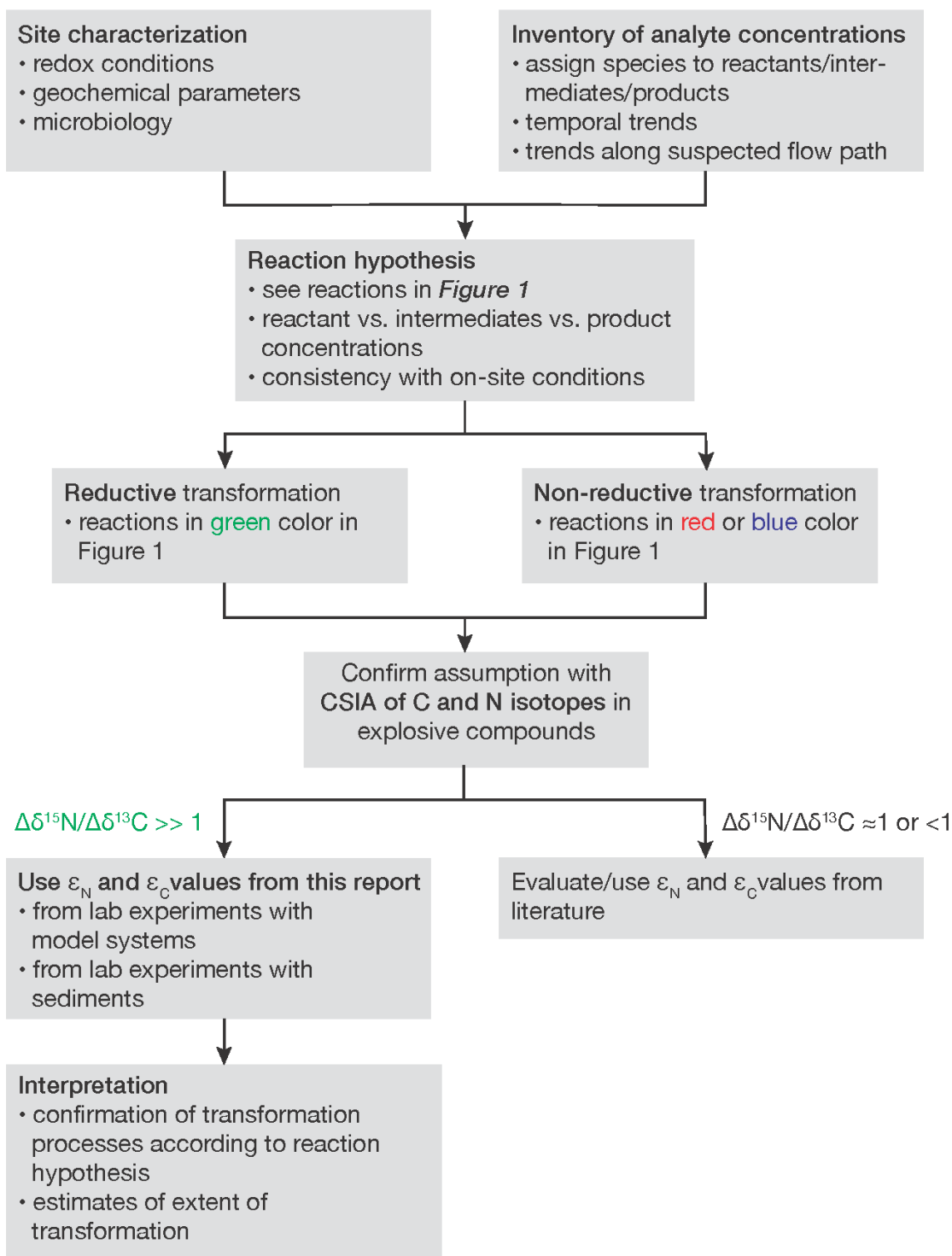


Figure 21. Proposed workflow for the use of CSIA to support identification of nitro explosive degradation reaction and estimation of the extent of transformation attributable to the specified reaction.

4 CONCLUSIONS AND RECOMMENDATIONS

Studies to date have shown that IRMS use for CSIA is a robust and accurate measurement tool when appropriate standardization, calibration and quality assurance/quality control measures are implemented. Laboratory experiments isolating individual reaction processes are needed to determine the enrichment factors for a given pollutant, but there are often similarities for molecules of similar structure for a given reaction pathway. To that end, isotopic enrichment factors with specific meaning for a contaminant can be deduced from the AKIE that is generally valid for a degradation process. For NACs and RDX, enrichment of a single element (either N or C) can be used to verify that transformation of a pollutant is occurring and assess the extent of transformation. For example, oxidation tends to lead to larger carbon enrichment with smaller effects of nitrogen, and reduction leads to large effects on nitrogen with minimal effects on carbon. Note that in NACs, the isotope effects for carbon isotopes are more diluted than those for nitrogen. Additional subtleties can be found based on the reactive site (e.g., enzymatic versus alkaline hydrolysis of DNAN). In some cases, although monitoring the fractionation of a single element may be sufficient, acquiring isotopic data for two elements (N and C for explosives) provides the ability to more definitively identify the reaction process occurring and evaluate if multiple reactions may be occurring simultaneously (e.g., hydrolysis and reduction).

To perform CSIA, there is currently a need for specialized equipment (and robust analytical quality assurance/quality control measures), but advances in high resolution mass spectrometry will likely lead to wider use of the technique. Sample collection, handling, and processing methodologies used for CSIA of water and solid samples are routine in most laboratories performing other analyses of environmental samples.

While CSIA provides key information as to whether a contaminant is being transformed, additional data from field samples is still needed as confirmatory evidence. Concentration data, when used with the isotope measurements, can be used to evaluate the importance of non-fractionating processes. If the concentration is smaller than that predicted by the isotopic enrichment, it may indicate that another, non-fractionating process (e.g., dilution) is also lowering the pollutant levels. Additionally, measurement of known reaction intermediates/products of abiotic or biological reactions, groundwater chemistry/redox conditions, and genomic/proteomic evidence for biodegradation provide important supporting information for verifying the specific reaction process occurring. A complicating factor in interpreting isotopic measurements is the potential masking of the signal due to transport or other limitations on the reaction.

To fully implement CSIA among the broad range of nitro explosives, additional laboratory measurements of isotope fractionation for various potential abiotic and biological reaction processes should continue to build the library of enrichment factors. Improvements in the analytical capabilities for RDX and NTO, and well as other nitro components of munitions, will

expand the utility of CSIA for assessment of attenuation of these species in groundwater and other matrices.

5 REFERENCES

- (1) Elsner, M. Stable Isotope Fractionation to Investigate Natural Transformation Mechanisms of Organic Contaminants: Principles, Prospects and Limitations. *Journal of Environmental Monitoring*. The Royal Society of Chemistry November 3, 2010, pp 2005–2031. <https://doi.org/10.1039/c0em00277a>.
- (2) Aelion, C. M.; Höhener, P.; Hunkeler, D.; Aravena, R. *Environmental Isotopes in Biodegradation and Bioremediation*; CRC Press, 2009. <https://doi.org/10.1201/9781420012613>.
- (3) Schmidt, T. C.; Zwank, L.; Elsner, M.; Berg, M.; Meckenstock, R. U.; Haderlein, S. B. Compound-Specific Stable Isotope Analysis of Organic Contaminants in Natural Environments: A Critical Review of the State of the Art, Prospects, and Future Challenges. *Analytical and Bioanalytical Chemistry*. Springer January 28, 2004, pp 283–300. <https://doi.org/10.1007/s00216-003-2350-y>.
- (4) Elsner, M.; Zwank, L.; Hunkeler, D.; Schwarzenbach, R. P. A New Concept Linking Observable Stable Isotope Fractionation to Transformation Pathways of Organic Pollutants. *Environ. Sci. Technol.* **2005**, 39 (18), 6896–6916. <https://doi.org/10.1021/es0504587>.
- (5) Hatzinger, P.; Koster Van Groos, P.; Fuller, M.; Sturchio, N. C. *Guidance for Using Compound Specific Isotope Analysis (CSIA) to Document the Biodegradation and Natural Attenuation of RDX Distribution Statement A*; 2019.
- (6) Wijker, R. S.; Bolotin, J.; F. Nishino, S.; C. Spain, J.; B. Hofstetter, T. Using Compound-Specific Isotope Analysis to Assess Biodegradation of Nitroaromatic Explosives in the Subsurface. *Environ. Sci. Technol.* **2013**, 47 (13), 6872–6883. <https://doi.org/10.1021/es3051845>.
- (7) Berg, M.; Bolotin, J.; Hofstetter, T. B. Compound-Specific Nitrogen and Carbon Isotope Analysis of Nitroaromatic Compounds in Aqueous Samples Using Solid-Phase Microextraction Coupled to GC/IRMS. *Anal. Chem.* **2007**, 79 (6), 2386–2393. <https://doi.org/10.1021/ac0622577>.
- (8) Brand, W. A.; Coplen, T. B.; Vogl, J.; Rosner, M.; Prohaska, T. Assessment of International Reference Materials for Isotope-Ratio Analysis (IUPAC Technical Report). In *Pure and Applied Chemistry*; IUPAC Secretariat, 2014; Vol. 86, pp 425–467. <https://doi.org/10.1515/pac-2013-1023>.
- (9) Schimmelmann, A.; Qi, H.; Coplen, T. B.; Brand, W. A.; Fong, J.; Meier-Augenstein, W.; Kemp, H. F.; Toman, B.; Ackermann, A.; Assonov, S.; et al. Organic Reference Materials for Hydrogen, Carbon, and Nitrogen Stable Isotope-Ratio Measurements: Caffeines, n-Alkanes, Fatty Acid Methyl Esters, Glycines, l -Valines, Polyethylenes, and Oils. *Anal. Chem.* **2016**, 88 (8), 4294–4302. <https://doi.org/10.1021/acs.analchem.5b04392>.
- (10) Schimmelmann, A.; Albertino, A.; Sauer, P. E.; Qi, H.; Molinie, R.; Mesnard, F. Nicotine, Acetanilide and Urea Multi-Level ² H-, ¹³ C- and ¹⁵ N-Abundance Reference Materials for

- Continuous-Flow Isotope Ratio Mass Spectrometry. *Rapid Commun. Mass Spectrom.* **2009**, 23 (22), 3513–3521. <https://doi.org/10.1002/rcm.4277>.
- (11) Wijker, R. S.; Kurt, Z.; Spain, J. C.; Bolotin, J.; Zeyer, J.; Hofstetter, T. B. Isotope Fractionation Associated with the Biodegradation of 2- and 4-Nitrophenols via Monooxygenation Pathways. *Environ. Sci. Technol.* **2013**, 47 (24), 14185–14193. <https://doi.org/10.1021/es403876u>.
- (12) Wijker, R. S.; Adamczyk, P.; Bolotin, J.; Paneth, P.; Hofstetter, T. B. Isotopic Analysis of Oxidative Pollutant Degradation Pathways Exhibiting Large H Isotope Fractionation. *Environ. Sci. Technol.* **2013**, 47 (23), 13459–13468. <https://doi.org/10.1021/es403597v>.
- (13) Ulrich, B. A.; Palatucci, M.; Bolotin, J.; Spain, J. C.; Hofstetter, T. B. Different Mechanisms of Alkaline and Enzymatic Hydrolysis of the Insensitive Munition Component 2,4-Dinitroanisole Lead to Identical Products. *Environ. Sci. Technol. Lett.* **2018**, 5 (7), 456–461. <https://doi.org/10.1021/acs.estlett.8b00258>.
- (14) Wang, C.; Wallace, A. F.; Heraty, L.; Qi, H.; Sturchio, N. C. Alkaline Hydrolysis Pathway of 2,4-Dinitroanisole Verified by ^{18}O Tracer Experiment. *J. Hazard. Mater.* **2020**, 396, 122627. <https://doi.org/10.1016/j.jhazmat.2020.122627>.
- (15) Fuller, M. E.; Koster van Groos, P. G.; Jarrett, M.; Kucharzyk, K. H.; Minard-Smith, A.; Heraty, L. J.; Sturchio, N. C. Application of a Multiple Lines of Evidence Approach to Document Natural Attenuation of Hexahydro-1,3,5-Trinitro-1,3,5-Triazine (RDX) in Groundwater. *Chemosphere* **2020**, 250, 126210. <https://doi.org/10.1016/j.chemosphere.2020.126210>.
- (16) Bernstein, A.; Adar, E.; Ronen, Z.; Lowag, H.; Stichler, W.; Meckenstock, R. U. Quantifying RDX Biodegradation in Groundwater Using $\Delta^{15}\text{N}$ Isotope Analysis. *J. Contam. Hydrol.* **2010**, 111 (1–4), 25–35. <https://doi.org/10.1016/j.jconhyd.2009.10.010>.
- (17) Bernstein, A.; Ronen, Z.; Adar, E.; Nativ, R.; Lowag, H.; Stichler, W.; Meckenstock, R. U. Compound-Specific Isotope Analysis of RDX and Stable Isotope Fractionation during Aerobic and Anaerobic Biodegradation. *Environ. Sci. Technol.* **2008**, 42 (21), 7772–7777. <https://doi.org/10.1021/es8005942>.
- (18) Sagi-Ben Moshe, S.; Ronen, Z.; Dahan, O.; Bernstein, A.; Weisbrod, N.; Gelman, F.; Adar, E. Isotopic Evidence and Quantification Assessment of in Situ RDX Biodegradation in the Deep Unsaturated Zone. *Soil Biol. Biochem.* **2010**, 42 (8), 1253–1262. <https://doi.org/10.1016/j.soilbio.2010.04.011>.
- (19) Godin, J.-P.; McCullagh, J. S. O. Review: Current Applications and Challenges for Liquid Chromatography Coupled to Isotope Ratio Mass Spectrometry (LC/IRMS). *Rapid Commun. Mass Spectrom.* **2011**, 25 (20), 3019–3028. <https://doi.org/10.1002/rcm.5167>.
- (20) Schilling, I. E.; Hess, R.; Bolotin, J.; Lal, R.; Hofstetter, T. B.; Kohler, H. P. E. Kinetic Isotope Effects of the Enzymatic Transformation of γ -Hexachlorocyclohexane by the Lindane Dehydrochlorinase Variants LinA1 and LinA2. *Environ. Sci. Technol.* **2019**, 53 (5), 2353–2363. <https://doi.org/10.1021/acs.est.8b04234>.
- (21) Berens, M. J.; Ulrich, B. A.; Strehlau, J. H.; Hofstetter, T. B.; Arnold, W. A. Mineral

- Identity, Natural Organic Matter, and Repeated Contaminant Exposures Do Not Affect the Carbon and Nitrogen Isotope Fractionation of 2,4-Dinitroanisole during Abiotic Reduction. *Environ. Sci. Process. Impacts* **2019**, *21* (1).
<https://doi.org/10.1039/c8em00381e>.
- (22) Spahr, S.; Huntscha, S.; Bolotin, J.; Maier, M. P.; Elsner, M.; Hollender, J.; Hofstetter, T. B. Compound-Specific Isotope Analysis of Benzotriazole and Its Derivatives. *Anal. Bioanal. Chem.* **2013**, *405* (9), 2843–2856. <https://doi.org/10.1007/s00216-012-6526-1>.
 - (23) Nair, S.; Geilmann, H.; Coplen, T. B.; Qi, H.; Gehre, M.; Schimmelmann, A.; Brand, W. A. Isotopic Disproportionation during Hydrogen Isotopic Analysis of Nitrogen-Bearing Organic Compounds. *Rapid Commun. Mass Spectrom.* **2015**, *29* (9), 878–884.
<https://doi.org/10.1002/rcm.7174>.
 - (24) Gelman, F.; Kotlyar, A.; Chiguala, D.; Ronen, Z. Precise and Accurate Compound-Specific Carbon and Nitrogen Isotope Analysis of RDX by GC-IRMS. *Int. J. Environ. Anal. Chem.* **2011**, *91* (14), 1392–1400. <https://doi.org/10.1080/03067319.2010.484888>.
 - (25) Fuller, M. E.; Heraty, L.; Condee, C. W.; Vainberg, S.; Sturchio, N. C.; Hatzinger, P. B. Relating Carbon and Nitrogen Isotope Effects to Reaction Mechanisms during Aerobic or Anaerobic Degradation of RDX (Hexahydro-1,3,5- Trinitro-1,3,5-Triazine) by Pure Bacterial Cultures Mark. *Appl. Environ. Microbiol.* **2016**, *82* (11), 3297–3309.
<https://doi.org/10.1128/AEM.00073-16.Editor>.
 - (26) Howa, J. D.; Lott, M. J.; Chesson, L. A.; Ehleringer, J. R. Carbon and Nitrogen Isotope Ratios of Factory-Produced RDX and HMX. *Forensic Sci. Int.* **2014**, *240* (2014), 80–87.
<https://doi.org/10.1016/j.forsciint.2014.04.013>.
 - (27) Julien, M.; Parinet, J.; Nun, P.; Bayle, K.; Höhener, P.; Robins, R. J.; Remaud, G. S. Fractionation in Position-Specific Isotope Composition during Vaporization of Environmental Pollutants Measured with Isotope Ratio Monitoring by ¹³C Nuclear Magnetic Resonance Spectrometry. *Environ. Pollut.* **2015**, *205*, 299–306.
<https://doi.org/10.1016/j.envpol.2015.05.047>.
 - (28) Julien, M.; Gori, D.; Höhener, P.; Robins, R. J.; Remaud, G. S. Intramolecular Isotope Effects during Permanganate Oxidation and Acid Hydrolysis of Methyl Tert-Butyl Ether. *Chemosphere* **2020**, *248*, 125975. <https://doi.org/10.1016/j.chemosphere.2020.125975>.
 - (29) Wang, C.; Heraty, L. J.; Wallace, A. F.; Liu, C.; Li, X.; McGovern, G. P.; Horita, J.; Fuller, M. E.; Hatzinger, P. B.; Sturchio, N. C. Position-Specific Isotope Effects during Alkaline Hydrolysis of 2,4-Dinitroanisole Resolved by Compound-Specific Isotope Analysis, ¹³C NMR, and Density-Functional Theory. *Chemosphere* **2021**, in revision.
 - (30) Eiler, J.; Cesar, J.; Chimiak, L.; Dallas, B.; Grice, K.; Griep-Raming, J.; Juchelka, D.; Kitchen, N.; Lloyd, M.; Makarov, A.; et al. Analysis of Molecular Isotopic Structures at High Precision and Accuracy by Orbitrap Mass Spectrometry. *Int. J. Mass Spectrom.* **2017**, *422*, 126–142. <https://doi.org/10.1016/j.ijms.2017.10.002>.
 - (31) Neubauer, C.; Sweredoski, M. J.; Moradian, A.; Newman, D. K.; Robins, R. J.; Eiler, J. M. Scanning the Isotopic Structure of Molecules by Tandem Mass Spectrometry. *Int. J. Mass Spectrom.* **2018**, *434*, 276–286. <https://doi.org/10.1016/j.ijms.2018.08.001>.

- (32) Coplen, T. B. Guidelines and Recommended Terms for Expression of Stable-Isotope-Ratio and Gas-Ratio Measurement Results. *Rapid Commun. Mass Spectrom.* **2011**, *25* (17), 2538–2560. <https://doi.org/10.1002/rcm.5129>.
- (33) Coleman, M.; Meier-Augenstein, W. Ignoring IUPAC Guidelines for Measurement and Reporting of Stable Isotope Abundance Values Affects Us All. *Rapid Commun. Mass Spectrom.* **2014**, *28* (17), 1953–1955. <https://doi.org/10.1002/rcm.6971>.
- (34) Reference Materials: Schimmelmann Research: Indiana University Bloomington <https://hcnisotopes.earth.indiana.edu/reference-materials/index.html> (accessed Mar 15, 2021).
- (35) Skrzypek, G. Normalization Procedures and Reference Material Selection in Stable HCNOS Isotope Analyses: An Overview. *Analytical and Bioanalytical Chemistry*. Springer March 8, 2013, pp 2815–2823. <https://doi.org/10.1007/s00216-012-6517-2>.
- (36) Dunn, P. J. H.; Hai, L.; Malinovsky, D.; Goenaga-Infante, H. Simple Spreadsheet Templates for the Determination of the Measurement Uncertainty of Stable Isotope Ratio Delta Values. *Rapid Commun. Mass Spectrom.* **2015**, *29* (22), 2184–2186. <https://doi.org/10.1002/rcm.7376>.
- (37) Jochmann, M. A.; Blessing, M.; Haderlein, S. B.; Schmidt, T. C. A New Approach to Determine Method Detection Limits for Compound-Specific Isotope Analysis of Volatile Organic Compounds. *Rapid Commun. Mass Spectrom.* **2006**, *20* (24), 3639–3648. <https://doi.org/10.1002/rcm.2784>.
- (38) Elsner, M.; Jochmann, M. A.; Hofstetter, T. B.; Hunkeler, D.; Bernstein, A.; Schmidt, T. C.; Schimmelmann, A. Current Challenges in Compound-Specific Stable Isotope Analysis of Environmental Organic Contaminants. *Anal. Bioanal. Chem.* **2012**, *403* (9), 2471–2491. <https://doi.org/10.1007/s00216-011-5683-y>.
- (39) Parnell, A. C.; Phillips, D. L.; Bearhop, S.; Semmens, B. X.; Ward, E. J.; Moore, J. W.; Jackson, A. L.; Grey, J.; Kelly, D. J.; Inger, R. Bayesian Stable Isotope Mixing Models. *Environmetrics* **2013**, *24* (6), n/a-n/a. <https://doi.org/10.1002/env.2221>.
- (40) Centler, F.; Heße, F.; Thullner, M. Estimating Pathway-Specific Contributions to Biodegradation in Aquifers Based on Dual Isotope Analysis: Theoretical Analysis and Reactive Transport Simulations. *J. Contam. Hydrol.* **2013**, *152*, 97–116. <https://doi.org/10.1016/j.jconhyd.2013.06.009>.
- (41) Eckert, D.; Rolle, M.; Cirpka, O. A. Numerical Simulation of Isotope Fractionation in Steady-State Bioreactive Transport Controlled by Transverse Mixing. *J. Contam. Hydrol.* **2012**, *140–141*, 95–106. <https://doi.org/10.1016/j.jconhyd.2012.08.010>.
- (42) Scott, K. M.; Lu, X.; Cavanaugh, C. M.; Liu, J. S. Optimal Methods for Estimating Kinetic Isotope Effects from Different Forms of the Rayleigh Distillation Equation. *Geochim. Cosmochim. Acta* **2004**, *68* (3), 433–442. [https://doi.org/10.1016/S0016-7037\(03\)00459-9](https://doi.org/10.1016/S0016-7037(03)00459-9).
- (43) Pati, S. G.; Kohler, H. P. E.; Hofstetter, T. B. Characterization of Substrate, Cosubstrate, and Product Isotope Effects Associated With Enzymatic Oxygenations of Organic

- Compounds Based on Compound-Specific Isotope Analysis. In *Methods in Enzymology*; Academic Press, 2017; Vol. 596, pp 291–329. <https://doi.org/10.1016/bs.mie.2017.06.044>.
- (44) Buchner, D.; Jin, B.; Ebert, K.; Rolle, M.; Elsner, M.; Haderlein, S. B. Experimental Determination of Isotope Enrichment Factors - Bias from Mass Removal by Repetitive Sampling. *Environ. Sci. Technol.* **2017**, *51* (3), 1527–1536. <https://doi.org/10.1021/acs.est.6b03689>.
- (45) Höhener, P.; Atteia, O. Rayleigh Equation for Evolution of Stable Isotope Ratios in Contaminant Decay Chains. *Geochim. Cosmochim. Acta* **2014**, *126*, 70–77. <https://doi.org/10.1016/j.gca.2013.10.036>.
- (46) Dorer, C.; Höhener, P.; Hedwig, N.; Richnow, H. H.; Vogt, C. Rayleigh-Based Concept to Tackle Strong Hydrogen Fractionation in Dual Isotope Analysis - The Example of Ethylbenzene Degradation by Aromatoleum Aromaticum. *Environ. Sci. Technol.* **2014**, *48* (10), 5788–5797. <https://doi.org/10.1021/es404837g>.
- (47) Tellinghuisen, J. Least-Squares Analysis of Data with Uncertainty in x and y: A Monte Carlo Methods Comparison. *Chemom. Intell. Lab. Syst.* **2010**, *103* (2), 160–169. <https://doi.org/10.1016/j.chemolab.2010.07.003>.
- (48) Ojeda, A. S.; Phillips, E.; Mancini, S. A.; Lollar, B. S. Sources of Uncertainty in Biotransformation Mechanistic Interpretations and Remediation Studies Using CSIA. *Anal. Chem.* **2019**, *91* (14), 9147–9153. <https://doi.org/10.1021/acs.analchem.9b01756>.
- (49) Tellinghuisen, J. Least-Squares Analysis of Data with Uncertainty in y and x: Algorithms in Excel and KaleidaGraph. *J. Chem. Educ.* **2018**, *95* (6), 970–977. <https://doi.org/10.1021/acs.jchemed.8b00069>.
- (50) Skarpeli-Liati, M.; Jiskra, M.; Turgeon, A.; Garr, A. N.; Arnold, W. A.; Cramer, C. J.; Schwarzenbach, R. P.; Hofstetter, T. B. Using Nitrogen Isotope Fractionation to Assess the Oxidation of Substituted Anilines by Manganese Oxide. *Environ. Sci. Technol.* **2011**, *45* (13). <https://doi.org/10.1021/es200743t>.
- (51) Pati, S. G.; Shin, K.; Skarpeli-Liati, M.; Bolotin, J.; Eustis, S. N.; Spain, J. C.; Hofstetter, T. B. Carbon and Nitrogen Isotope Effects Associated with the Dioxygenation of Aniline and Diphenylamine. *Environ. Sci. Technol.* **2012**, *46* (21), 11844–11853. <https://doi.org/10.1021/es303043t>.
- (52) Berens, M. J.; Hofstetter, T. B.; Bolotin, J.; Arnold, W. A. Assessment of 2,4-Dinitroanisole Transformation Using Compound-Specific Isotope Analysis after In Situ Chemical Reduction of Iron Oxides. *Environ. Sci. Technol.* **2020**, *54* (9), 5520–5531. <https://doi.org/10.1021/acs.est.9b07616>.
- (53) Tong, Y.; Berens, M. J.; Ulrich, B. A.; Bolotin, J.; Strehlau, J. H.; Hofstetter, T. B.; Arnold, W. A. Exploring the Utility of Compound-Specific Isotope Analysis for Assessing Ferrous Iron-Mediated Reduction of RDX in the Subsurface. *ChemRxiv*. ChemRxiv December 11, 2020. <https://doi.org/10.26434/chemrxiv.13366316.v1>.
- (54) Sviatenko, L.; Kinney, C.; Gorb, L.; C. Hill, F.; J. Bednar, A.; Okovytyy, S.; Leszczynski, J. Comprehensive Investigations of Kinetics of Alkaline Hydrolysis of TNT (2,4,6-

- Trinitrotoluene), DNT (2,4-Dinitrotoluene), and DNAN (2,4-Dinitroanisole). *Environ. Sci. Technol.* **2014**, *48* (17), 10465–10474. <https://doi.org/10.1021/es5026678>.
- (55) Bernstein, A.; Ronen, Z.; Gelman, F. Insight on RDX Degradation Mechanism by Rhodococcus Strains Using ¹³C and ¹⁵N Kinetic Isotope Effects. *Environ. Sci. Technol.* **2013**, *47* (1), 479–484. <https://doi.org/10.1021/es302691g>.
 - (56) Hofstetter, T. B.; Neumann, A.; Arnold, W. A.; Hartenbach, A. E.; Bolotin, J.; Cramer, C. J.; Schwarzenbach, R. P. Substituent Effects on Nitrogen Isotope Fractionation during Abiotic Reduction of Nitroaromatic Compounds. *Environ. Sci. Technol.* **2008**, *42* (6), 1997–2003. <https://doi.org/10.1021/es702471k>.
 - (57) Hartenbach, A.; Hofstetter, T. B.; Berg, M.; Bolotin, J.; Schwarzenbach, R. P. Using Nitrogen Isotope Fractionation to Assess Abiotic Reduction of Nitroaromatic Compounds. *Environ. Sci. Technol.* **2006**, *40* (24), 7710–7716. <https://doi.org/10.1021/es061074z>.
 - (58) Hofstetter, T. B.; Schwarzenbach, R. P.; Bernasconi, S. M. Assessing Transformation Processes of Organic Compounds Using Stable Isotope Fractionation. *Environ. Sci. Technol.* **2008**, *42* (21), 7737–7743. <https://doi.org/10.1021/es801384j>.
 - (59) Berens, M. J.; Ulrich, B. A.; Strehlau, J. H.; Hofstetter, T. B.; Arnold, W. A. Mineral Identity, Natural Organic Matter, and Repeated Contaminant Exposures Do Not Affect the Carbon and Nitrogen Isotope Fractionation of 2,4-Dinitroanisole during Abiotic Reduction. *Environ. Sci. Process. Impacts* **2019**, *21* (1), 51–62. <https://doi.org/10.1039/c8em00381e>.
 - (60) Wang, C.; Fuller, M. E.; Heraty, L. J.; Hatzinger, P. B.; Sturchio, N. C. Photocatalytic Mechanisms of 2,4-Dinitroanisole Degradation in Water Deciphered by C and N Dual-Element Isotope Fractionation. *J. Hazard. Mater.* **2021**, *411*, 125109. <https://doi.org/10.1016/j.jhazmat.2021.125109>.
 - (61) Tobler, N. B.; Hofstetter, T. B.; Schwarzenbach, R. P. Assessing Iron-Mediated Oxidation of Toluene and Reduction of Nitroaromatic Contaminants in Anoxic Environments Using Compound-Specific Isotope Analysis. *Environ. Sci. Technol.* **2007**, *41* (22), 7773–7780. <https://doi.org/10.1021/es071129c>.
 - (62) Hunkeler, D.; Meckenstock, R. U.; Lollar, B. S.; Schmidt, T. C.; Wilson, J. T. A Guide for Assessing Biodegradation and Source Identification of Organic Ground Water Contaminants Using Compound Specific Isotope Analysis (CSIA). *U.S. Environ. Prot. Agency* **2008**, *EPA/600/R-* (December), 1–82.
 - (63) Sherwood Lollar, B.; Slater, G. F.; Sleep, B.; Witt, M.; Klecka, G. M.; Harkness, M.; Spivack, J. Stable Carbon Isotope Evidence for Intrinsic Bioremediation of Tetrachloroethene and Trichloroethene at Area 6, Dover Air Force Base. *Environ. Sci. Technol.* **2001**, *35* (2), 261–269. <https://doi.org/10.1021/es001227x>.
 - (64) US Army Corp of Engineers, Groundwater Flow and Contaminant Fate and Transport Modeling Line 800 Pink Water Lagoon, Iowa Army Ammunition Plant, Middletown, Iowa.

Ref	Reference - see Tab 3
NAC	Compound identity - see below
IsExplosive	TRUE for explosives, FALSE for other NACs
system	identity of reactive species.
type	abiotic or biological reaction
Isotope	identify of element for which fractionation is measured
eps	enrichment factor
eps_err	reported error for enrichment factor
AKIE	apparent kinetic isotope effect
AKIE_err	reported error for apparent kinetic isotope effect
redox	identification of reaction as oxidation or reduction.

12DNB	1,2-dinitrobenzene
14DNB	1,4-dinitrobenzene
24DNT	2,4-dinitrotoluene
26DNT	2,6-dinitrotoluene
2CINB	2-chloronitrobenzene
2NP	2-nitrophenol
2NT	2-nitrotoluene
3CINB	3-chloronitrobenzene
3NP	3-nitrophenol
3NT	3-nitrotoluene
4CINB	4-chloronitrobenzene
4NT	4-nitrotoluene
5-CH3-2NP	5-methyl-2-nitrophenol
DNAN	dinitroanisole
NB	nitrobenzene
RDX	1,3,5-trinitro-1,3,5-triazine
TNT	trinitrotoluene

Ref	NAC	IsExplosive	system	type	Isotope	eps	eps_err	AKIE	AKIE_err	redox
1	12DNB	TRUE	AH2QDS	abiotic	N	-13.6	0.1	1.0281	0.0003	reduction
1	12DNB	TRUE	AH2QDS	abiotic	N	-5.3	0.5	1.0107	0.001	reduction
5	12DNB	TRUE	CBD/SWa-1	abiotic	N	-17.4	0.8	1.0361	0.0017	reduction
5	14DNB	TRUE	CBD/SWa-1	abiotic	N	-17.3	0.9	1.0358	0.0019	reduction
7	24DNT	TRUE	bio	biological	N	-1.2	0.2			oxidation
7	24DNT	TRUE	bio	biological	C	-0.5	0.2			oxidation
7	24DNT	TRUE	bio	biological	H	-7.5	1.2			oxidation
10	26DNT	TRUE	bio	biological	C	-1.1	0.4	1.008	0.003	oxidation
10	26DNT	TRUE	bio	biological	H	-21	4	1.128	0.029	oxidation
1	2CINB	FALSE	AH2QDS	abiotic	N	-37.1	0.4	1.0385	0.0004	reduction
2	2CINB	FALSE	Fe(II)/goethite	abiotic	N	-29.2	0.3	1.0301	0.0003	reduction
2	2CINB	FALSE	juglone/H2S	abiotic	N	-30.2	1.7	1.0312	0.0017	reduction
5	2CINB	FALSE	CBD/SWa-1	abiotic	N	-38.3	3.2	1.0398	0.0033	reduction
8	2NP	FALSE	bio	biological	N	-1.4	0.2	1.0014	0.0001	oxidation
8	2NP	FALSE	bio	biological	C	-1.2	0.1	1.007	0.0007	oxidation
8	2NP	FALSE	bio	biological	C	-1.4	0.1	1.0086	0.0008	oxidation
1	2NT	TRUE	AH2QDS	abiotic	N	-43.3	0.3	1.0453	0.0003	reduction
1	2NT	TRUE	AH2QDS	abiotic	N	-38.9	0.8	1.0405	0.0009	reduction
1	2NT	TRUE	AH2QDS	abiotic	N	-37.7	1	1.0392	0.0011	reduction
1	2NT	TRUE	AH2QDS	abiotic	N	-38.1	0.8	1.0396	0.0008	reduction
1	2NT	TRUE	AH2QDS	abiotic	N	-40.5	0.7	1.0423	0.0008	reduction
1	2NT	TRUE	AH2QDS	abiotic	N	-40.2	0.4	1.0419	0.0004	reduction
1	2NT	TRUE	AH2QDS	abiotic	N	-41.2	0.7	1.0429	0.0007	reduction
1	2NT	TRUE	AH2QDS	abiotic	N	-41.3	0.5	1.0431	0.0006	reduction
1	2NT	TRUE	AH2QDS	abiotic	N	-43.1	0.8	1.045	0.0008	reduction
1	2NT	TRUE	AH2QDS	abiotic	N	-41.9	0.3	1.0438	0.0003	reduction
1	2NT	TRUE	AH2QDS	abiotic	N	-39.1	0.8	1.0407	0.0008	reduction
1	2NT	TRUE	AH2QDS	abiotic	N	-39.5	0.5	1.0412	0.0005	reduction
1	2NT	TRUE	AH2QDS	abiotic	N	-17.1	0.3	1.0354	0.0007	reduction
2	2NT	TRUE	Fe(II)/goethite	abiotic	N	-31.9	1	1.0329	0.001	reduction
5	2NT	TRUE	CBD/SWa-1	abiotic	N	-37.7	2.3	1.0392	0.0024	reduction
9	2NT	TRUE	bio	biological	N	-1.6	0.2			oxidation
9	2NT	TRUE	bio	biological	C	-1.3	0.1	1.023	0.002	oxidation
9	2NT	TRUE	bio	biological	C	-1.2	0.3			oxidation
10	2NT	TRUE	bio	biological	C	-1.3	0.1	1.018	0.001	oxidation
10	2NT	TRUE	bio	biological	C	-0.4	0.1	1.004	0.001	oxidation
10	2NT	TRUE	bio	biological	H	-4.6	2			oxidation
10	2NT	TRUE	bio	biological	H	-3.5	0.6			oxidation
5	3CINB	FALSE	CBD/SWa-1	abiotic	N	-39.9	1.6	1.0416	0.0016	reduction
6	3CINB	FALSE	Fe(II)/goethite	abiotic	N	-39	1	1.406	0.001	reduction
6	3CINB	FALSE	Fe(II)/goethite	abiotic	N	-40.6	0.9	1.0423	0.001	reduction
6	3CINB	FALSE	Fe(II)/goethite	abiotic	N	-40.3	2	1.042	0.0022	reduction
6	3CINB	FALSE	Fe(II)/goethite	abiotic	N	-36.6	1.2	1.038	0.0013	reduction
6	3CINB	FALSE	Fe(II)/goethite	abiotic	N	-38.7	1.3	1.0403	0.0014	reduction
6	3CINB	FALSE	Fe(II)/goethite	abiotic	N	-41.6	0.8	1.0434	0.0009	reduction
6	3CINB	FALSE	Fe(II)/goethite	abiotic	N	-41.9	1.1	1.0437	0.0012	reduction
6	3CINB	FALSE	Fe(II)/goethite	abiotic	N	-32.9	0.7	1.034	0.0007	reduction
8	3NP	FALSE	bio	biological	N	-22	0.2	1.0224	0.0002	reduction
8	3NP	FALSE	bio	biological	N	-22	0.4	1.0226	0.0004	reduction
8	3NP	FALSE	bio	biological	C	-0.3	0.1	1.0003	0.0001	reduction
8	3NP	FALSE	bio	biological	C	-0.3	0.2	1.0003	0.0001	reduction
10	3NT	FALSE	bio	biological	C	-0.4	0.2	1.01	0.001	oxidation
10	3NT	FALSE	bio	biological	C	-0.6	0.2	1.004	0.001	oxidation
10	3NT	FALSE	bio	biological	H	-2.6	1.6	1.019	0.012	oxidation
10	3NT	FALSE	bio	biological	H	-5.9	0.7			oxidation
1	4CINB	FALSE	AH2QDS	abiotic	N	-40.3	0.6	1.042	0.0006	reduction
1	4CINB	FALSE	tiron	abiotic	N	-34.6	1.3	1.0358	0.0013	reduction
1	4CINB	FALSE	tiron	abiotic	N	-30.3	1.3	1.0312	0.0013	reduction
1	4CINB	FALSE	tiron	abiotic	N	-28.1	0.4	1.0289	0.0004	reduction
1	4CINB	FALSE	tiron	abiotic	N	-20.7	1.6	1.0212	0.0016	reduction
1	4CINB	FALSE	tiron	abiotic	N	-13.3	3	1.0135	0.003	reduction
1	4CINB	FALSE	tiron	abiotic	N	-12.1	0.5	1.0122	0.0005	reduction
1	4CINB	FALSE	tiron	abiotic	N	-13.7	1.2	1.0139	0.0012	reduction
1	4CINB	FALSE	tiron	abiotic	N	-41.2	4.4	1.0429	0.0044	reduction
1	4CINB	FALSE	tiron	abiotic	N	-17.5	1.3	1.0178	0.0013	reduction
2	4CINB	FALSE	Fe(II)/goethite	abiotic	N	-29.4	0.8	1.0303	0.0008	reduction
2	4CINB	FALSE	juglone/H2S	abiotic	N	-28	0.8	1.0288	0.0008	reduction

5	4CINB	FALSE	CBD/SWa-1	abiotic	N	-39.6	0.8	1.0412	0.0009	reduction
6	4CINB	FALSE	Fe(II)/goethite	abiotic	N	-31.1	1	1.0321	0.0011	reduction
7	4CINB	FALSE	Fe(II)/goethite	abiotic	N	-29.4	0.8			reduction
7	4CINB	FALSE	Fe(II)/goethite	abiotic	C	-0.7	0.1			reduction
1	4NT	FALSE	AH2QDS	abiotic	N	-40.4	0.2	1.0421	0.0002	reduction
2	4NT	FALSE	Fe(II)/goethite	abiotic	N	-31.3	1.4	1.0324	0.0014	reduction
5	4NT	FALSE	CBD/SWa-1	abiotic	N	-38.7	1.5	1.0402	0.0006	reduction
7	4NT	FALSE	bio	biological	N	-25.3	0.8			reduction
7	4NT	FALSE	bio	biological	C	-0.6	0.2			reduction
10	4NT	FALSE	bio	biological	C	-1.4	0.4	1.01	0.002	oxidation
10	4NT	FALSE	bio	biological	C	-0.1	0.1	1.003	0.001	oxidation
7	4NT	FALSE	bio	biological	H	-9.9	2.2			reduction
7	4NT	FALSE	bio	biological	H	-111	4			oxidation
10	4NT	FALSE	bio	biological	H	-5.5	2.3			oxidation
10	4NT	FALSE	bio	biological	H	-2.6	1.1			oxidation
8	5-CH3-2NP	FALSE	bio	biological	N	0.8	0.1	1.0042	0.0001	oxidation
8	5-CH3-2NP	FALSE	bio	biological	N	0.9	0.1	1.0014	0.0001	oxidation
8	5-CH3-2NP	FALSE	bio	biological	C	-1.3	0.1	1.0092	0.0005	oxidation
8	5-CH3-2NP	FALSE	bio	biological	C	-1.5	0.1	1.0102	0.0004	oxidation
3	DNAN	TRUE	mackinawite	abiotic	N	-19	1	1.039	0.001	reduction
3	DNAN	TRUE	mackinawite	abiotic	N	-16	1	1.034	0.001	reduction
3	DNAN	TRUE	mackinawite	abiotic	N	-16	2	1.034	0.002	reduction
3	DNAN	TRUE	Fe(II)/goethite	abiotic	N	-17	3	1.035	0.003	reduction
3	DNAN	TRUE	Fe(II)/goethite	abiotic	N	-16	5	1.034	0.005	reduction
3	DNAN	TRUE	Fe(II)/goethite	abiotic	N	-11	1	1.022	0.001	reduction
3	DNAN	TRUE	Fe(II)/magnetite	abiotic	N	-15	4	1.031	0.003	reduction
3	DNAN	TRUE	Fe(II)/magnetite	abiotic	N	-17	3	1.036	0.003	reduction
3	DNAN	TRUE	Fe(II)/magnetite	abiotic	N	-9	2	1.01	0.002	reduction
4	DNAN	TRUE	Fe(II)/Tinker	abiotic	N	-11.1	4.3	1.023	0.009	reduction
4	DNAN	TRUE	Fe(II)/hematite	abiotic	N	-21.2	3.3	1.044	0.007	reduction
4	DNAN	TRUE	Fe(II)/TCAAP	abiotic	N	-21.5	2.6	1.045	0.005	reduction
4	DNAN	TRUE	Fe(II)/magnetite	abiotic	N	-13.2	1.7	1.027	0.003	reduction
4	DNAN	TRUE	Dithionite/Tinker	abiotic	N	-9.9	3.8	1.02	0.008	reduction
4	DNAN	TRUE	Dithionite/TCAAP	abiotic	N	-15.8	4.3	1.033	0.009	reduction
13	DNAN	TRUE	alkaline hydrolysis	abiotic	N	-2.7	0.4	1.0027	0.0004	oxidation
13	DNAN	TRUE	bio	biological	N	-2.5	0.1	1.0025	0.0001	hydrolysis
13	DNAN	TRUE	bio	biological	N	-3.2	0.1	1.0032	0.0003	hydrolysis
3	DNAN	TRUE	mackinawite	abiotic	C	-0.8	0.6	1.0008	0.0008	reduction
3	DNAN	TRUE	mackinawite	abiotic	C	-0.7	1.4	1.0007	0.0014	reduction
3	DNAN	TRUE	mackinawite	abiotic	C	-1.5	1.2	1.0015	0.0012	reduction
3	DNAN	TRUE	Fe(II)/goethite	abiotic	C	-0.1	0.3	1	0.0003	reduction
3	DNAN	TRUE	Fe(II)/goethite	abiotic	C	-0.6	0.4	1.006	0.0004	reduction
3	DNAN	TRUE	Fe(II)/goethite	abiotic	C	-1.2	0.9	1.0012	0.0009	reduction
3	DNAN	TRUE	Fe(II)/magnetite	abiotic	C	-0.7	0.6	1.0007	0.0006	reduction
3	DNAN	TRUE	Fe(II)/magnetite	abiotic	C	-1.3	0.2	1.0013	0.0005	reduction
3	DNAN	TRUE	Fe(II)/magnetite	abiotic	C	-0.1	0.2	1	0.0002	reduction
4	DNAN	TRUE	Fe(II)/Tinker	abiotic	C	-0.7	0.1	1.0007	0.0002	reduction
4	DNAN	TRUE	Fe(II)/hematite	abiotic	C	-0.3	0.4	1.0003	0.0008	reduction
4	DNAN	TRUE	Fe(II)/TCAAP	abiotic	C	-0.8	1	1.0008	0.002	reduction
4	DNAN	TRUE	Fe(II)/magnetite	abiotic	C	-0.7	0.3	1.0007	0.0006	reduction
4	DNAN	TRUE	Dithionite/Tinker	abiotic	C	-0.2	0.1	1.0002	0.0002	reduction
4	DNAN	TRUE	Dithionite/TCAAP	abiotic	C	-0.3	0.2	1.0003	0.0004	reduction
13	DNAN	TRUE	alkaline hydrolysis	abiotic	C	-6	0.5	1.044	0.003	
13	DNAN	TRUE	bio	biological	C	-2.8	0.1	1.02	0.003	oxidation
13	DNAN	TRUE	bio	biological	C	-3.7	0.1	1.027	0.005	oxidation
	DNAN	TRUE	alkaline hydrolysis	abiotic	C	-5.46	0.15			
	DNAN	TRUE	alkaline hydrolysis	abiotic	C	-5.98	0.17			
	DNAN	TRUE	alkaline hydrolysis	abiotic	C	-6.52	0.37			
	DNAN	TRUE	alkaline hydrolysis	abiotic	N	-3.08	0.1			
	DNAN	TRUE	alkaline hydrolysis	abiotic	N	-3.35	0.16			
	DNAN	TRUE	alkaline hydrolysis	abiotic	N	-2.59	0.17			
7	NB	FALSE	bio	biological	N	-0.8	0.1			
7	NB	FALSE	bio	biological	N	-26.6	0.7			reduction
9	NB	FALSE	bio	biological	N	-1	0.3	1.001	0.001	oxidation
9	NB	FALSE	bio	biological	N	-0.8	0.3	1.001	0.001	oxidation
12	NB	FALSE	bio	biological	N	-0.75	0.09	1.0008	0.0001	oxidation
12	NB	FALSE	bio	biological	N	-26.6	0.7	1.0273	0.0008	reduction
7	NB	FALSE	bio	biological	C	-3.9	0.1			oxidation

7 NB	FALSE	bio	biological	C	-0.6	0.1			reduction
9 NB	FALSE	bio	biological	C	-3.5	0.2	1.021	0.001	oxidation
9 NB	FALSE	bio	biological	C	-3.9	0.2	1.024	0.001	oxidation
9 NB	FALSE	bio	biological	C	-3.7	0.2	1.022	0.002	oxidation
9 NB	FALSE	bio	biological	C	-3.6	0.3			oxidation
10 NB	FALSE	bio	biological	C	-3.7	0.2	1.025	0.001	oxidation
10 NB	FALSE	bio	biological	C	-0.8	0.2	1.005	0.001	oxidation
12 NB	FALSE	bio	biological	C	-3.9	0.09	1.0241	0.0005	oxidation
12 NB	FALSE	bio	biological	C	-0.57	0.06	1.0034	0.0003	reduction
7 NB	FALSE	bio	biological	H	-6.3	0.5			oxidation
10 NB	FALSE	bio	biological	H	-5.6	1.2	1.027	0.0008	oxidation
10 NB	FALSE	bio	biological	H	-3.4	1.2	1.017	0.006	oxidation
14 RDX	TRUE	bio	biological	N	-2.3	0.8			reduction
14 RDX	TRUE	bio	biological	N	-2.3	0.8			reduction
14 RDX	TRUE	bio	biological	N	-1.9	0.4			reduction
14 RDX	TRUE	bio	biological	N	-1.9	0.3			reduction
14 RDX	TRUE	bio	biological	N	-2.1	0.1			reduction
14 RDX	TRUE	alkaline hydrolysis	abiotic	N	-5.3	0.8			oxidation
15 RDX	TRUE	bio	biological	N	-9.6	1.3			reduction
15 RDX	TRUE	bio	biological	N	-5.8	2.6			reduction
15 RDX	TRUE	bio	biological	N	-10.9	1.2			reduction
15 RDX	TRUE	bio	biological	N	-8	5.5			reduction
15 RDX	TRUE	bio	biological	N	-13.3	1.5			reduction
15 RDX	TRUE	bio	biological	N	-12.7	1.1			reduction
15 RDX	TRUE	bio	biological	N	-2.8	0.5			oxidation
15 RDX	TRUE	bio	biological	N	-2.6	0.3			oxidation
15 RDX	TRUE	bio	biological	N	-2.3	0.4			oxidation
15 RDX	TRUE	bio	biological	N	-2.3	0.5			oxidation
16 RDX	TRUE	alkaline hydrolysis	abiotic	N	-5.3				oxidation
11 RDX	TRUE	bio	biological	C	-2.1	0.1			oxidation
11 RDX	TRUE	bio	biological	C	-5	0.3			oxidation
14 RDX	TRUE	bio	biological	C	0.86	0.84			reduction
14 RDX	TRUE	alkaline hydrolysis	abiotic	C	-7.8	0.5			oxidation
15 RDX	TRUE	bio	biological	C	-6	2.6			reduction
15 RDX	TRUE	bio	biological	C	-4.1	1.6			reduction
15 RDX	TRUE	bio	biological	C	-2	0.5			reduction
15 RDX	TRUE	bio	biological	C	-2.8	1.6			reduction
15 RDX	TRUE	bio	biological	C	-3.1	1			reduction
15 RDX	TRUE	bio	biological	C	-2.1	1.3			reduction
15 RDX	TRUE	bio	biological	C	-1.3	2.3			oxidation
15 RDX	TRUE	bio	biological	C	0.3	0.8			oxidation
15 RDX	TRUE	bio	biological	C	-0.7	0.3			oxidation
15 RDX	TRUE	bio	biological	C	-0.9	0.6			oxidation
16 RDX	TRUE	alkaline hydrolysis	abiotic	C	-7.8				oxidation
1 TNT	TRUE	AH2QDS	abiotic	N	-8.6	0.4	1.0265	0.0011	reduction
1 TNT	TRUE	AH2QDS	abiotic	N	-3.4	0.2	1.01	0.0005	reduction

Ref

- ¹ Hartenbach, A. E.; Hofstetter, T. B.; Aeschbacher, M.; Sander, M.; Kim, D.; Strathmann, T. J.; Arnold, W. A.; Cramer, C. J.; Schwarzenbach, R. P. Variability of Nitrogen Isotope Fractionation during the Reduction of Nitroaromatic Compounds with Dissolved Reductants. *Environmental Science & Technology* 2008, 42 (22), 8352–8359. <https://doi.org/10.1021/es011933u>.
- ² Hartenbach, A.; Hofstetter, T. B.; Berq, M.; Bolotin, J.; Schwarzenbach, R. P. Using Nitrogen Isotope Fractionation to Assess Abiotic Reduction of Nitroaromatic Compounds. *Environmental science & technology* 2006, 40 (24), 7710–7716. <https://doi.org/10.1021/es061074z>.
- ³ Berens, M. J.; Ulrich, B. A.; Strehlau, J. H.; Hofstetter, T. B.; Arnold, W. A. Mineral Identity, Natural Organic Matter, and Repeated Contaminant Exposures Do Not Affect the Carbon and Nitrogen Isotope Fractionation of 2,4-Dinitroanisole during Abiotic Reduction. *Environmental Science: Processes & Impacts* 2018, 21, 51–62. <https://doi.org/10.1039/C6EM00381E>.
- ⁴ Berens, M. J.; Hofstetter, T. B.; Bolotin, J.; Arnold, W. A. Assessment of 2,4-Dinitroanisole Transformation Using Compound-Specific Isotope Analysis after In Situ Chemical Reduction of Iron Oxides. *Environmental Science & Technology* 2020, 54 (9), 5520–5531. <https://doi.org/10.1021/acs.est.9b07616>.
- ⁵ Hofstetter, T. B.; Neumann, A.; Arnold, W. A.; Hartenbach, A. E.; Bolotin, J.; Cramer, C. J.; Schwarzenbach, R. P. Substituent Effects on Nitrogen Isotope Fractionation during Abiotic Reduction of Nitroaromatic Compounds. *Environmental Science & Technology* 2008, 42 (6), 1997–2003. <https://doi.org/10.1021/es702471k>.
- ⁶ Tobler, N. B.; Hofstetter, T. B.; Schwarzenbach, R. P. Assessing Iron-Mediated Oxidation of Toluene and Reduction of Nitroaromatic Contaminants in Anoxic Environments Using Compound-Specific Isotope Analysis. *Environmental Science & Technology* 2007, 41 (22), 7773–7780. <https://doi.org/10.1021/es071129c>.
- ⁷ Wijker, R. S.; Bolotin, J.; Nishino, S. F.; Spain, J. C.; Hofstetter, T. B.; S. Wijker, R.; Bolotin, J.; F. Nishino, S.; C. Spain, J.; B. Hofstetter, T. Using Compound-Specific Isotope Analysis to Assess Biodegradation of Nitroaromatic Explosives in the Subsurface. *Environmental Science & Technology* 2013, 47 (13), 6872–6883. <https://doi.org/10.1021/es305184s>.
- ⁸ Wijker, R. S.; Zeyer, J.; Hofstetter, T. B. Isotope Fractionation Associated with the Simultaneous Biodegradation of Multiple Nitrophenol Isomers by *Pseudomonas Putida* B2. *Environmental Science: Processes & Impacts* 2017, 19 (5), 775–784. <https://doi.org/10.1039/C6EM00668J>.
- ⁹ Pati, S. G.; Kohler, H. P. E.; Bolotin, J.; Perales, R. E.; Hofstetter, T. B. Isotope Effects of Enzymatic Dioxygenation of Nitrobenzene and 2-Nitrotoluene by Nitrobenzene Dioxygenase. *Environmental Science & Technology* 2014, 48 (18), 10750–10759. <https://doi.org/10.1021/es5028844>.
- ¹⁰ Pati, S. G.; Kohler, H.-P. E.; Pabis, A.; Paneth, P.; Perales, R. E.; Hofstetter, T. B. Substrate and Enzyme Specificity of the Kinetic Isotope Effects Associated with the Dioxygenation of Nitroaromatic Contaminants. *Environmental Science & Technology* 2016, 50 (13), 6708–6716. <https://doi.org/10.1021/acs.est.5b05084>.
- ¹¹ Bernstein, A.; Ronen, Z.; Adar, E.; Nativ, R.; Lowag, H.; Stichler, W.; Meckenstock, R. U. Compound-Specific Isotope Analysis of RDX and Stable Isotope Fractionation during Aerobic and Anaerobic Biodegradation. *Environmental Science & Technology* 2008, 42 (21), 7772–7777. <https://doi.org/10.1021/es8005942>.
- ¹² Hofstetter, T. B.; Spain, J. C.; Nishino, S. F.; Bolotin, J.; Schwarzenbach, R. P.; B. Hofstetter, T.; C. Spain, J.; F. Nishino, S.; Bolotin, J.; P. Schwarzenbach, R. Identifying Competing Aerobic Nitrobenzene Biodegradation Pathways by Compound-Specific Isotope Analysis. *Environmental Science & Technology* 2006, 42 (13), 4764–4770. <https://doi.org/10.1021/es001053>.
- ¹³ Ulrich, B. A.; Palascucci, M.; Bolotin, J.; Spain, J. C.; Hofstetter, T. B. Different Mechanisms of Alkaline and Enzymatic Hydrolysis of the Insensitive Munition Component 2,4-Dinitroanisole Lead to Identical Products. *Environmental Science & Technology Letters* 2018, 5 (7), 456–461. <https://doi.org/10.1021/acs.estlett.8b00258>.
- ¹⁴ Bernstein, A.; Ronen, Z.; Gelman, F. Insight on RDX Degratation Mechanism by Rhodococcus Strains Using ¹³C and ¹⁵N Kinetic Isotope Effects. *Environmental Science & Technology* 2012, 47 (1), 479–484. <https://doi.org/10.1021/es302691a>.
- ¹⁵ Fuller, M. E.; Heraty, L.; Condée, C. W.; Vainberg, S.; Sturchio, N. C.; Hatzinger, P. B. Relating Carbon and Nitrogen Isotope Effects to Reaction Mechanisms during Aerobic or Anaerobic Degradation of RDX (Hexahydro-1,3,5- Trinitro-1,3,5-Triazine) by Pure Bacterial Cultures Mark. *Applied and Environmental Microbiology* 2016, 82 (11), 3297–3309. <https://doi.org/10.1128/AEM.00073-16>.Editor.
- ¹⁶ Gelman, F.; Kotlyar, A.; Chiuaila, D.; Ronen, Z. Precise and Accurate Compound-Specific Carbon and Nitrogen Isotope Analysis of RDX by GC-IRMS. *International Journal of Environmental Analytical Chemistry* 2011, 91 (14), 1392–1400. <https://doi.org/10.1080/03067319.2010.484888>.